PERIODICO di MINERALOGIA
established in 1930

DIPARTIMENTO
DI SCIENZE DELLA TERRA

SAPIENZA
UNIVERSITÀ DI ROMA

An International Journal of
Mineralogy, Crystallography, Geochemistry,
Ore Deposits, Petrology, Volcanology
and applied topics on Environment, Archaeometry and Cultural Heritage

Polymineralic hydrothermal veins in the Paleozoic Jandaq ophiolite gabbros (Central Iran); Evidence for ingression of high temperature seawater-derived fluids in to the gabbroic section of the Paleo-Tethys oceanic crust

Nargess Nosouhian [a], Ghodrat Torabi [a,*], Tomoaki Morishita [b], Shoji Arai [c]

[a] Department of Geology, University of Isfahan, Isfahan, 8174673441, Iran
[b] School of Natural System, College of Science and Engineering, Kanazawa University, 920-1192 Kanazawa, Japan
[c] Institute of Liberal Arts and Science, Kanazawa University, 920-1192 Kanazawa, Japan

ARTICLE INFO

Submitted: April 2022
Accepted: July 2022
Available on line: July 2022

* Corresponding author:
Torabighodrat@sci.ui.ac.ir

Doi: 10.13133/2239-1002/17725

How to cite this article:
Nosouhian N. et al. (2022)
Period. Mineral. 91, 113-142

ABSTRACT

The Paleozoic Jandaq ophiolite is situated in the western part of the Central-East Iranian microcontinent and is a remnant of the Paleo-Tethys oceanic crust. This ophiolite consists of mantle peridotites and serpentinized mantle peridotites, metagabbro, basic and ultrabasic metamorphosed dykes and lavas, metapyroxenite, amphibolite, rodingite and listwaenite which are covered by the Late Paleozoic schist and marble. The open spaces of joints and cracks of gabbroic dykes and stocks are filled by hydrothermal minerals such as calcite, prehnite, garnet (grossular-andradite), epidote, clinopyroxene (diopside), chlorite, albite and sericite. The calcite and garnet are the latest minerals in this association. The most predominant mineral is calcite with coarse-grained morphology. The main textures are granoblastic and poikiloblastic.

The very low abundances of Al, Ti, Na, Cr and rare earth elements (REEs) in clinopyroxenes support their metamorphic origin. The high modal abundance of calcite, the presence of clinopyroxene, garnet, prehnite and epidote as the Ca-bearing minerals, as well as the positive anomaly of Eu in the chondrite-normalized REE patterns of minerals possibly point to the seawater- derived penetrating fluids ingression through the oceanic crust-covering sediments and the uppermost portion of oceanic crust into the gabbros. The involved fluids in the Jandaq area have leached the calcite-bearing sediments (e.g., limestone) and calcic plagioclase-rich lithologies (e.g., basic pillow lavas and sheeted dykes) before reaching to the gabbros, caused to the CO_2, calcium and Eu enrichment of fluids. Accordingly, the hydrothermal veins in the Jandaq ophiolite are possibly formed by high temperature circulation of seawater-originated fluids throughout the uppermost oceanic crust.

Keywords: Gabbro; Hydrothermal vein; Seawater; Paleozoic; Jandaq ophiolite.

INTRODUCTION

Mass transfer between the seawater and the underlying oceanic lithosphere is considered as a first-order mechanism of chemical exchange (e.g., Alt, 1995; Staudigel et al., 1996). Metasomatic transport can be driven by fluid flow and by diffusion in the boundary metasomatism (e.g., Ferry and Dipple, 1991; Bach et al., 2012). The fluid percolates down in fissures and cracks of the oceanic crust is seawater (McCollom and Shock, 1998; Bach et al., 2012). Seawater circulation within the upper portion of the oceanic lithosphere is a process that modifies the composition of oceanic crust and seawater

(Bach et al., 2012; Harris et al., 2015).

Metasomatism due to interaction of circulating hydrothermal fluids with rocks from the oceanic lithosphere is an important process for control of crust-ocean chemical compositions, where the oceanic crust undergoes extensive chemical exchange with seawater from ridge to trench (Bach et al., 2012). Although the overall exchange fluxes are great, the first-order metasomatic changes of crustal rocks are usually <10% relative change in major element concentrations (e.g., Python et al., 2007a; Bach et al., 2012). The metasomatic mass transfers of major elements are developed only where high fluid fluxes and high temperature fluids prevail in the basaltic oceanic crust. Fluid pathways and temperatures affect the chemical composition of the fluids and their potential for element transport. The composition of seawater-derived crustal fluids quickly changes with increasing volumes of rock under high temperatures (Bach et al., 2012). One of the most important changes is the loss of Mg and sulfate, while Ca and silica concentrations increase in the mid and lower crustal rocks (i.e., sheeted dikes and gabbros) (e.g., Alt, 1995; Gillis, 1995; Dick et al., 2000; Python et al., 2007a; Bach et al., 2012). This process indicates that the hydrothermal alteration can be considered as a cation exchange process. The rates of chemical exchange are strongly dependent on temperature. Alkalis elements, B and C are removed from circulating fluids at temperatures <150 ^{o}C, but they are leached from the interacting rocks at higher temperatures (Staudigel et al., 1996; Jarrard, 2003). CO_2 is added to the oceanic crust, while carbonates are limited to the uppermost part of this crust (e.g., Staudigel et al., 1996).

The main factors controlling the mineral assemblages in fluid-rock interactions are temperature, pressure, the primary rock composition, as well as the chemical composition and mass flux of the fluid entering the rock (Bach et al., 2012). Petrological and geochemical researches reveal that hydrothermal fluids related to seawater ingression can reach and affect the base of sheeted dykes, gabbroic section and uppermost mantle (e.g., Berger et al., 2005; Python et al., 2007 a,b; Akizawa et al., 2011; Arai and Akizawa, 2014; Torabi et al., 2017). In the mantle-crust transition zone, the hydrothermal fluids lose the alkali elements by precipitation of minerals like amphibole, epidote, albite in hydrothermal veins. These fluids are selectively enriched in elements like Ca and Eu, due to their interaction with the gabbros from the lower crust (e.g., Python et al., 2007 a,b). The extent and the intensity of the hydrothermal metamorphism decrease downward. The published data about hydrothermal metamorphism by percolating seawater in the oceanic crust extended the depth of seawater circulation and metamorphism to the uppermost mantle (e.g., Python et al., 2007a, 2011; Akizawa et al., 2011; Akizawa and Arai, 2014; Arai and Akizawa, 2014; Torabi et al., 2017).

The main structural units of Iran and surrounding areas comprise of separated continental blocks. The formation and evolution of these blocks were controlled by the opening and closure of the Paleo-Tethys and Neo-Tethys oceans (e.g., Aistov et al., 1984; Bagheri, 2007; Shafaii Moghadam and Stern, 2014). The remnants of the Paleo-Tethys Ocean are preserved in southwestern Eurasia in Iran, Turkey, Caucasus, Turkmenistan, Afghanistan and Tibet (e.g., Lippard et al., 1986; Berra et al., 2017). Paleozoic (Davoudzadeh and Lensch, 1986; Davoudzadeh, 1997; Bagheri and Stampfli, 2008) successions related to the Paleo-Tethys Ocean occur in the south of the Great Kavir Fault, western part of Central-East Iranian Microcontinent (CEIM) (Figure 1). The CEIM is located between the Arabian and Eurasian plates and surrounded by major faults and Mesozoic (Upper Cretaceous to Lower Eocene) ophiolites that are remnants of the Neo-Tethys Ocean (Aistov et al., 1984; Davoudzadeh, 1997; Shafaii Moghadam and Stern, 2014; Figure 1). This microcontinent consists of four major blocks from east to the west; Lut, Tabas (Kerman), Posht-e-Badam, and Yazd (Naein) blocks (e.g., Takin, 1972; Alavi, 1991), which are separated by major faults and distinct horst (e.g., Lut block) and graben (e.g., Kerman-Tabas region) structures (e.g., Alavi, 1991; Almasian, 1997; Reichert, 2007). The CEIM blocks drifted from Gondwana and accreted to Eurasia as the result of northward subduction and closure of Paleo-Tethys in Permo-Triassic time (e.g., Berberian and King, 1981; Stampfli, 2000; Shafaii Moghadam and Stern, 2014; Rossetti et al., 2015; Shafaii Moghadam et al., 2020).

The Paleozoic ophiolites present good exposures in the north of Iran, consist of Mashhad and Rasht (Rossetti et al., 2017) and in the western part of the CEIM, comprising the Anarak, Jandaq, Bayazeh and Posht-e-Badam ophiolites (Nosouhian et al., 2014; 2019; Figure 1). They have suffered the sub-solidus evolutions, hydrothermal alteration and regional metamorphism (Nosouhian et al., 2019). Metagabbros are from the main constituents. Metagabbros in the Jandaq ophiolite have many joints and cracks filled by hydrothermal minerals. This research is the first study on the hydrothermal alteration of metagabbros in the Paleozoic ophiolites of Central Iran. Both hydrothermal veins and host metagabbros are studied. Results of this study reveal that hydrothermal fluids related to seawater ingression into the oceanic crust can reach and affect the gabbro section after penetration through basalts and sheeted dykes during spreading of the oceanic crust.

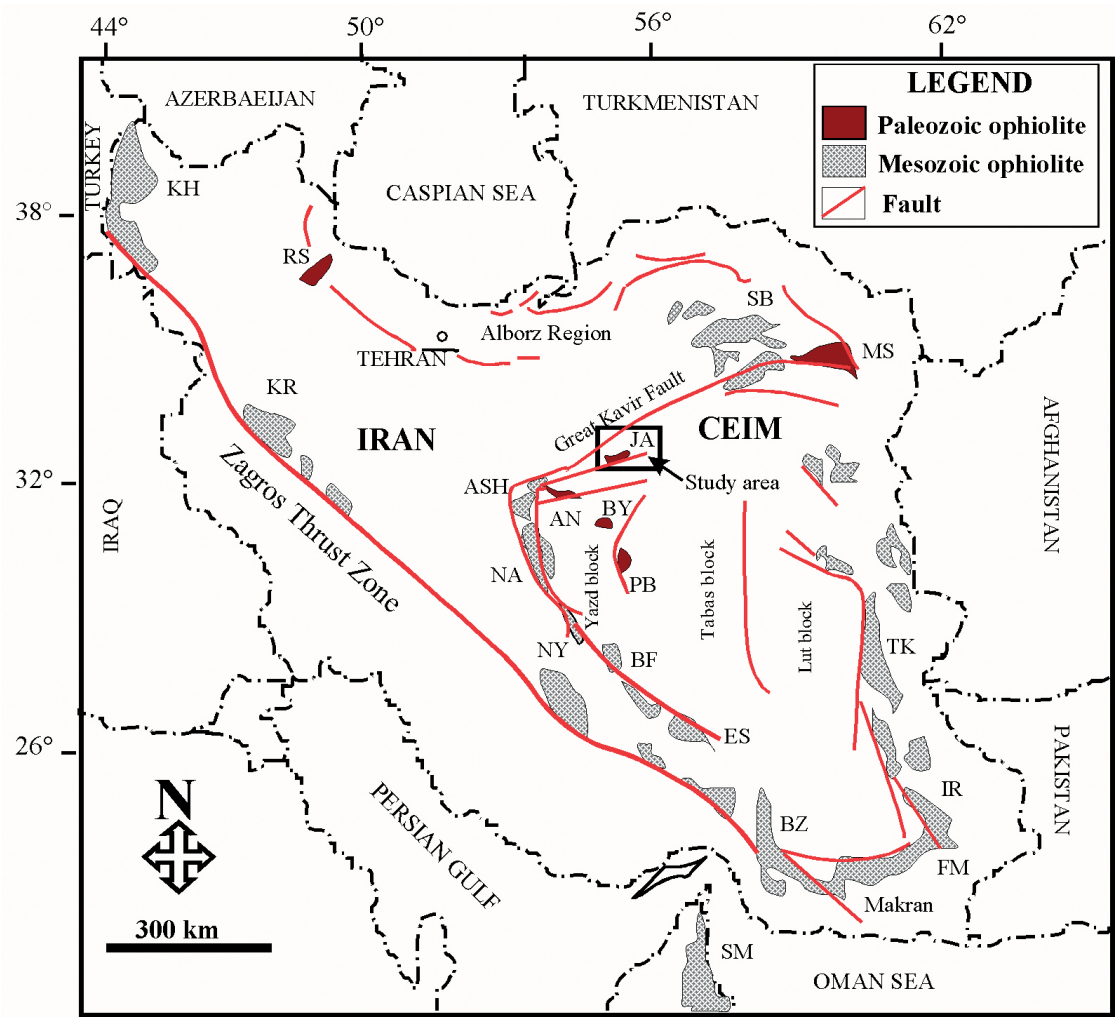

Figure 1. The main ophiolites of Iran (Torabi et al., 2011; slightly modified). KH= Khoy; KR= Kermanshah; NY= Neyriz; BZ= Band Ziarat; NA= Naein; BF= Baft; ES= Esphandagheh; FM= Fanuj-Maskutan; IR= Iranshahr; TK= TchehelKureh; MS= Mashhad; SB= Sabzevar; RS= Rasht; SM= Samail; ASH= Ashin; AN= Anarak; JA= Jandaq; BY= Bayazeh; PB= Posht-e-Badam.

GEOLOGICAL SETTING

Based on the evolution of the CEIM including the study area, the Anarak, Jandaq, Bayazeh and Posht-e-Badam ophiolites are likely related to the initial opening and subduction of the Paleo-Tethys Ocean (Bagheri and Stampfli, 2008; Torabi et al., 2011; Nosouhian, 2016; 2019; Figure 1). These ophiolites suggest a progression from oceanic crust formation above a subduction zone in Devonian time to accretionary convergence in Permian time (Bagheri, 2007). These Paleozoic ophiolites of Iran were emplaced when N-directed subduction resulted in collision of Gondwana fragment with Eurasia in Permo-Triassic time (e.g., Bagheri, 2007 and reference in it). After closure, the molasse sediments of Jurassic covered most of them (Bagheri and Stampfli, 2008). The Jandaq ophiolite and other Iranian Paleozoic ophiolites are mainly associated with flysch, turbidites and high pressure metamorphic rocks (Bagheri, 2007; Shafaii Moghadam and Stern, 2014; Torabi, 2011; Torabi and Arai, 2013). Based on the stratigraphic and palaeobiogeographic affinities, the succession at Jandaq significantly differs in terms of lithology from the Central Iran successions (Berra et al., 2017), mostly because it records a proximal siliciclastic input related to a nearby active margin, associated with Carboniferous metamorphism (Bagheri and Stampfli, 2008), pre-dating the deposition of the Pennsylvanian conglomerates (Shafaii Moghadam and Stern, 2014). Accordingly, the Jandaq succession has no similarity with the coeval succession of Central Iran and the Alborz, whereas it shows some similarities with the Paleozoic successions of Fariman and Aghdarband (Shafaii Moghadam and Stern, 2014). Previous studies

suggested a post-Triassic 135° anti-clockwise rotation of the Central Iran transferring a large fragment of the Paleo-Tethys suture from the present-day Afghanistan-Iran border to Central Iran (e.g., Davoudzadeh, 1997). But, the palaeomagnetic data of the Nakhlak Triassic succession by Muttoni et al. (2009), Late Triassic palaeomagnetic data of Besse et al. (1998), fauna studies by Balini et al. (2009), and regional facies analysis of Upper Silurian-Lower Carboniferous successions by Wendt et al. (2005), do not support this idea. However, the occurrence of Paleozoic ophiolites in the western part of the CEIM propounds many questions about the evolution and the number of Paleo-Tethys sutures between Eurasian and Iran (Zanchi et al., 2009). The presence of Paleozoic ophiolites along the main faults of central and northern Iran possibly point to a multi-suture closure of the Paleo-Tethys Ocean in Late Paleozoic to Early Mesozoic times (e.g., Torabi et al., 2011). The final collision between the Gondwana and Eurasia occurred in Triassic time with the Eocimmerian collision (Bagheri and Stampfli, 2008). The Jandaq area presents all the elements of an orogen such as dismembered ophiolites and deformed siliciclastic, calcareous and volcanic rocks (Bagheri and Stampfli, 2008).

The lithological and chemical characteristics of ophiolitic complexes can provide useful information about the tectonic setting of their formation. Ophiolites can originate in mid-ocean ridge (MOR) and supra-subduction zone (SSZ) tectonic settings (e.g., Van Hinsbergen et al., 2015 and references therein). The Iranian Paleozoic ophiolites show both SSZ- and MORB-type mineralogical and geochemical signatures. The most of the Paleozoic ophiolites of Iran are formed in back-arc basins (Bagheri, 2007; Shafaii Moghadam and Stern, 2014). The geological history of the CEIM confirm a SSZ (back-arc) setting for the ophiolitic mélange with Paleozoic age in the Yazd block including the Anarak, Jandaq, Bayazeh and Posht-e-Badam ophiolites (Bagheri, 2007; Bagheri and Stampfli, 2008).

The Paleozoic Jandaq ophiolite consists of mantle peridotites and serpentinized mantle peridotites, metagabbro, basic and ultrabasic metamorphosed dikes and lavas, metapyroxenite, amphibolite, rodingite and listwaenite. Mantle peridotites are composed of metalherzolite and metaharzburgite (Torabi et al., 2011). This ophiolite has been covered by the Paleozoic metamorphic rocks such as schist and marble (Figure 2). Middle Jurassic granite and mylonitic granite intrusions cross-cut the Jandaq ophiolite and the covering metamorphic rocks (Figure 2). Sandstone, siltstone and conglomerate of the Upper Jurassic Chahpalang formation, together with the Cretaceous limestones, cover the Jandaq ophiolite, associated metamorphic rocks and granitic intrusions (Figure 2). ^{40}Ar-^{39}Ar isotopic analyses on hornblende from amphibolites of the Jandaq ophiolite (156.56±33.15 Ma) and on muscovite in micaschist (163.86±1.76 Ma) possibly point to the Middle Jurassic metamorphism and the Middle Cimmerian orogeny (e.g.,

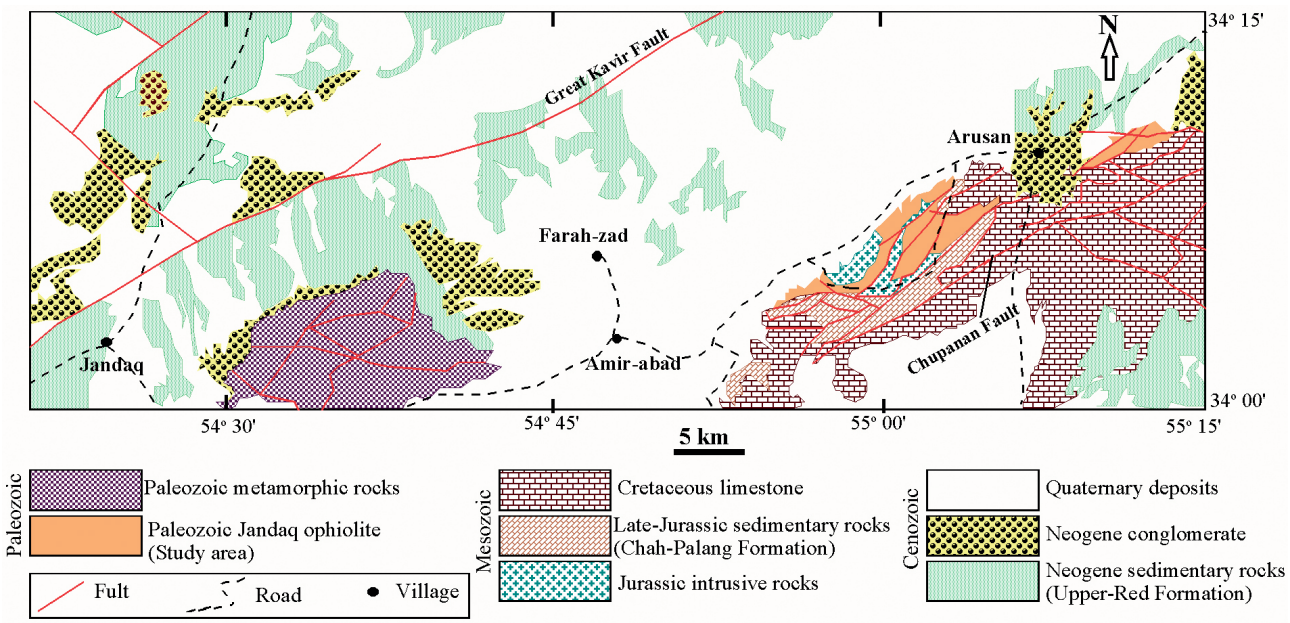

Figure 2. Simplified geological map of the Jandaq area in the western part of the Central-East Iranian Microcontinent (Yazd block) and position of the study area (modified after Aistov et al., 1984).

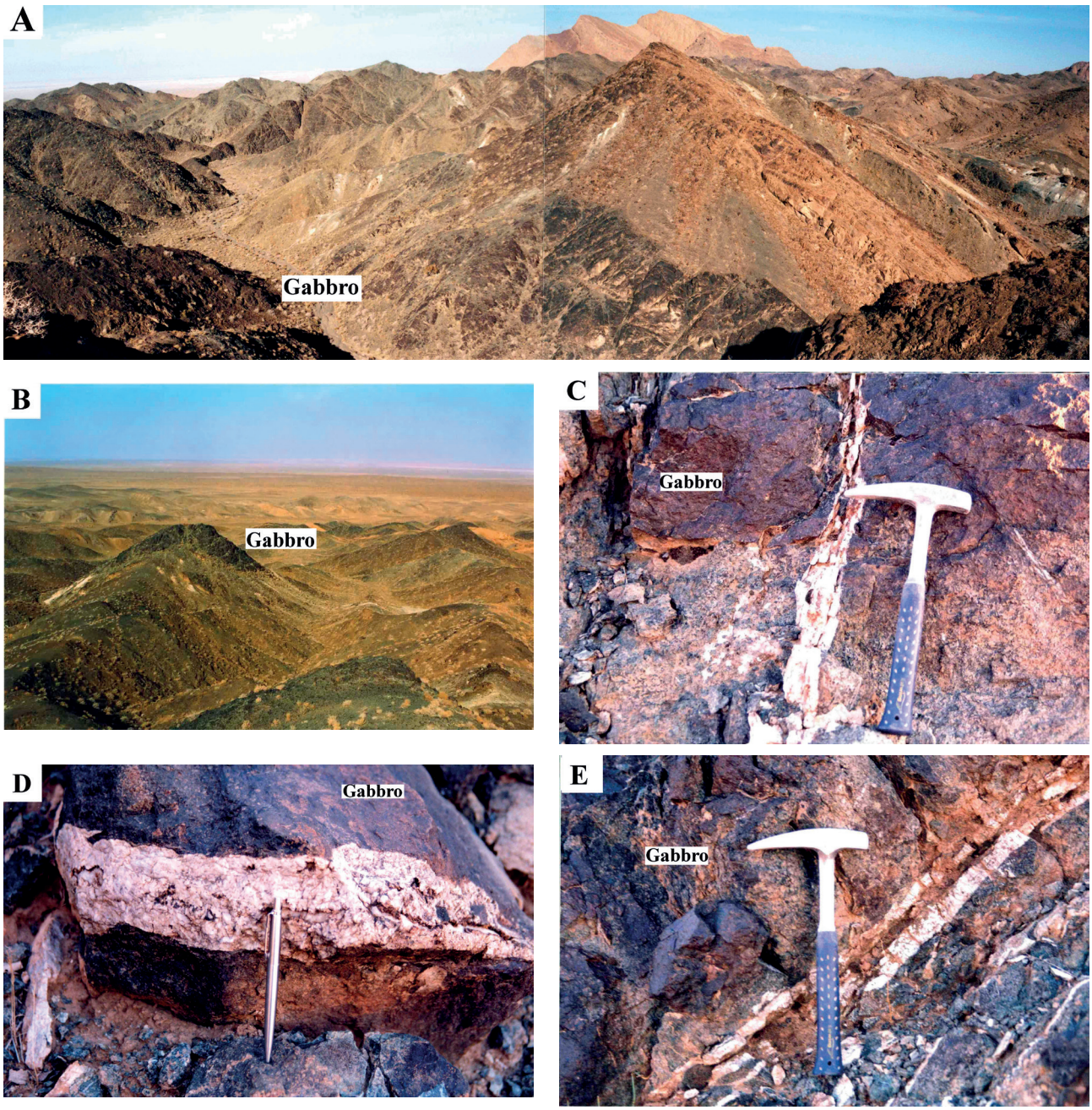

Figure 3. Field photos of the Jandaq area; (A,B) General view of the Jandaq ophiolite. (C,D,E) Metagabbros and the studied hydrothermal veins.

Bagheri, 2007; Nosouhian et al., 2016).

The metagabbros of the Jandaq ophiolite present hard exposures in the field, and are more resistant to erosion relative to the surrounding metaperidotites (Figure 3 A,B). These metagabbros are mainly exposed as massive, black to dark grey and coarse-grained rocks (Figure 3C). The Joints and cracks appear as dyke-like structures within the metagabbros (Figure 3 C,D,E). The hydrothermal veins filled these former cracks. The studied veins have sharp contacts with the surrounding metagabbros (Figure 3 C,D,E). The samples of these hydrothermal veins are coarse-grained in the hand specimen. The studied veins are homogeneous in color, white in general, but show green spots in outcrops. The white parts are essentially composed of calcite and diopside, whereas the green spots are mainly composed of garnet minerals.

The studied hydrothermal veins are found only in the gabbro section of the Jandaq ophiolite (Figure 3). It is possibly indicates that the former cracks eventually are filled by crystallization products of the fluids that circulated the host gabbros and overlying rock units. The width and length of these hydrothermal veins reach up to 35 centimeters and 5 meters, respectively (Figure 3 D,E).

ANALYTICAL METHODS

Chemical composition of minerals in the Jandaq ophiolite metagabbros and hydrothermal veins were measured at the School of Natural System, College of Science and Engineering, Kanazawa University (Kanazawa, Japan) using a wavelength dispersive electron probe microanalyzer (EPMA) (JEOL JXA-8800R). Analyses was performed under an accelerating voltage of 20 kV, a probe current of 20 nA, and a focused beam diameter of 3μm. The ZAF program was used for data correction. The Fe^{3+} and Fe^{2+} contents of minerals were calculated by assuming mineral stoichiometry (Droop, 1987). Chemical composition of natural minerals and synthetic materials were used as standards. The Mg# and Fe^{2+}# of minerals calculated as $Mg/(Mg+Fe^{2+})$ and $Fe^{2+}/(Mg+Fe^{2+})$ of atomic ratios, respectively. Representative chemical analyses of minerals and their calculated structural formula are listed in Tables 1 to 8.

The trace element compositions of minerals from the Jandaq metagabbros and hydrothermal veins were determined by laser ablation system (193 nm ArF excimer: Geolas Q-Plus, MicroLas) coupled to an Agilent 7500s ICP-MS system at the Kanazawa University, Japan (Morishita et al., 2005). The diameter of the analyzed points was 110 μm at 10 Hz with energy density of 8 J/cm^2 per pulse. Chemical analyses of minerals carried out by LA-ICP-MS are presented in Table 9. Mineral abbreviations in the tables and photomicrographs are from Whitney and Evans (2010). The abbreviations of labradorite, andesine and oligoclase are Lab, Ande and Olig in tables, respectively.

RESULTS

Petrography

The Jandaq metagabbros are composed of plagioclase and amphibole as the major minerals with modal values of 45-50 vol% and 30-35 vol%, respectively (Figure 4 A,B). Epidote, chlorite, ilmenite, magnetite, calcite, titanite, biotite, muscovite and sericite are the minor minerals. These metagabbros mainly present granoblastic, nematoblastic and poikiloblastic textures (Figure 4 A,B). The alterations of plagioclases lead to the formation of actinolite, albite, calcite, epidote and chlorite (Figure 4B). Also, the sub-sea floor metamorphism has changed some of the primary calcic plagioclases into the secondary sodic ones. Some of the amphiboles are partly altered to the chlorite, titanite and magnetite (Figure 4 A,B).

The joints and cracks of the studied metagabbros are filled by mainly coarse-grained white minerals (Figure 3, 4). Mineral association of the contact zone between the hydrothermal veins and the metagabbros consists of plagioclase, amphibole and clinopyroxene as the major minerals and prehnite, epidote, garnet, sericite, calcite and magnetite as the minor minerals. Plagioclase is partly changed to the prehnite and chlorite. The modal value of clinopyroxene in the contact zone is more than its abundance in the core of veins. Granoblastic, poikiloblastic, nematoblastic and porphyroblastic are the main textures in this zone (Figure 4 C,D). Amphibole occurs in both metagabbro and contact zone. Petrographic studies show that three types of amphiboles are present in these rocks: (1) granular amphiboles which occur as the isolated grains in the metagabbros. These brown to greenish brown amphiboles are associated with the plagioclase and Fe-Ti oxides (Figure 4 A,B); (2) amphibole rims on the clinopyroxenes of the contact zone. These amphiboles have acicular shape and green color (Figure 4C); (3) brown to green amphibole pseudomorphs in the contact zone which completely or partly enclosed the clinopyroxene grains (Figure 4D).

The core sections of the hydrothermal veins are nearly homogeneous in the petrography and consist of calcite, garnet and prehnite, without the accessory phases (Figure 4 G,H). Calcite with coarse morphology is the main mineral. Garnet and calcite are the latest minerals in this association. The main textures in the core of veins are granoblastic and poikiloblastic (Figure 4 E,F). The hydrothermal veins are generally devoid of oxide and sulphide minerals.

Mineral chemistry

Major elements

Electron microprobe analyses of the various minerals in the Jandaq hydrothermal veins and enclosing metagabbros are presented in Tables 1 to 8. Feldspar and amphibole are present in both metagabbro and contact zone. The electron microprobe analyses of the feldspars in the metagabbros show chemical heterogeneity. Plagioclases are labradorite (An 50 to 63%), andesine (An 32 to 49%), oligoclase (An 21 to 25%) and albite (An 0 to 1%) (Table 1 and Figure 5A) in composition. Chemical compositions of the plagioclases in the contact zone are andesine (An 33 to 38%), oligoclase (An 15 to 28%) and albite (An 0 to 9%; Table 1, Figure 5A). Alkali feldspars with anorthoclase composition (An 7 to 8%) are present in the contact zone (Figure 5A).

Amphiboles are calcic and have a wide range of chemical compositions (Table 2; Figure 5B). They are

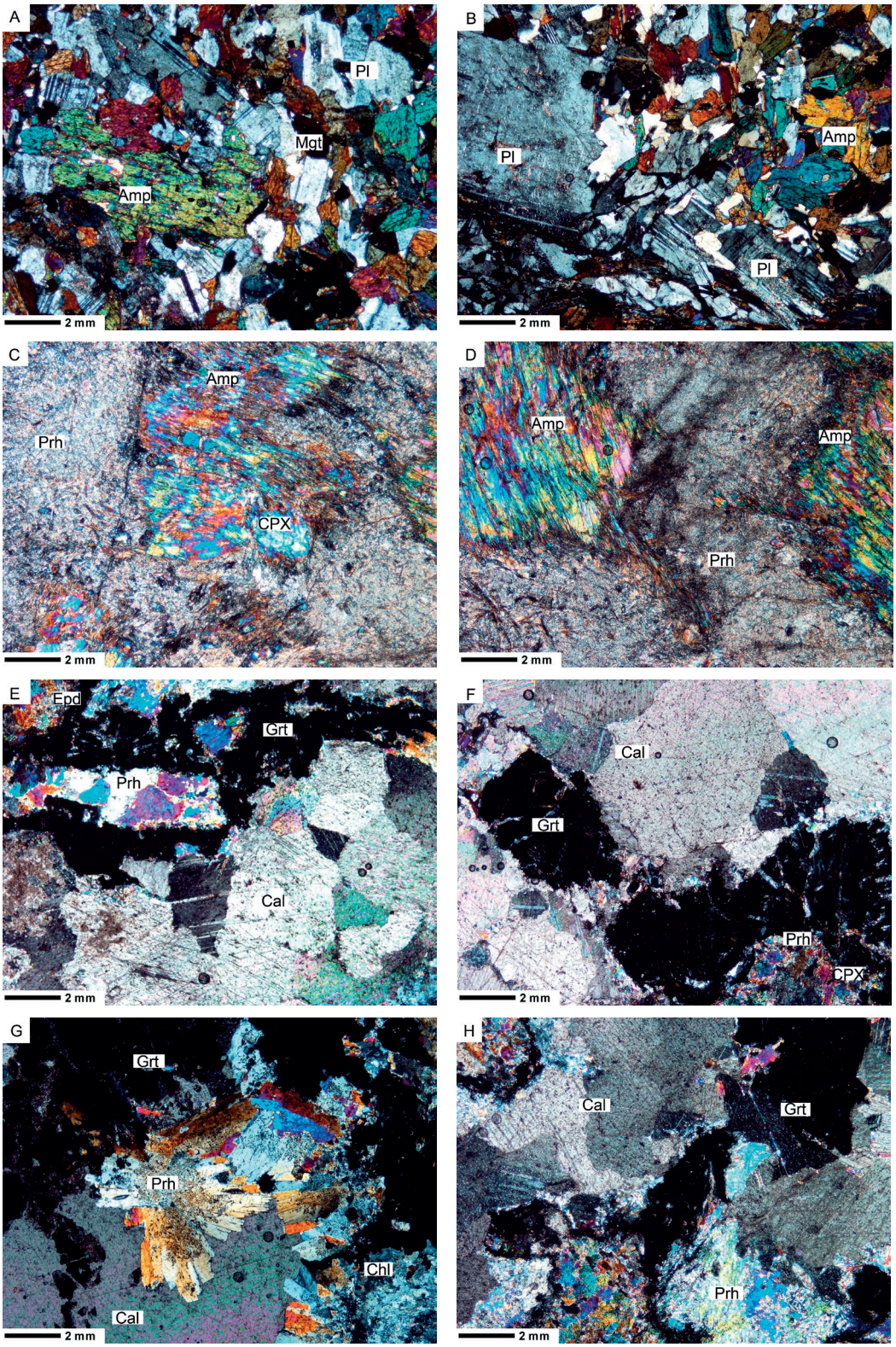

Figure 4. Photomicrographs of the Paleozoic Jandaq metagabbros and the hydrothermal veins. (A,B) Plagioclase and amphibole present mainly granoblastic, nematoblastic and poikiloblastic textures in the Jandaq metagabbros. (C,D) Contact zone between the metagabbros and veins mainly consists of albite, amphibole, prehnite, clinopyroxene and garnet. (E,F,G,H) Hydrothermal veins are composed of calcite, prehnite, garnet, epidote and clinopyroxene.

Table 1. Representative chemical compositions of feldspars (in wt.%) from the Jandaq ophiolite metagabbros and the contact zone (between the metagabbros and hydrothermal veins) and their calculated structural formula.

Rock type	Metagabbro																		
Sample no.	699	699	640	760	624	624	628	629	634	640	624-1	760	760	763	763	633	629	763	763
Point no.	209	215	49	191	25	27	29	37	42	51	61	179	182	194	201	31	35	198	206
Mineral	Ab	Ab	Olig	Olig	Ande	Ande	Ande	Ande	Ande	Ande	Ande	Ande	Ande	Ande	Ande	Lab	Lab	Lab	Lab
SiO_2	68.77	68.47	60.45	61.73	55.93	55.68	60.03	55.31	58.79	57.26	58.40	56.73	59.94	55.73	55.61	54.52	54.92	55.06	52.51
TiO_2	0.00	0.00	0.02	0.00	0.00	0.00	0.00	0.02	0.00	0.00	0.01	0.00	0.00	0.00	0.00	0.00	0.00	0.00	0.00
Al_2O_3	19.22	19.19	24.92	24.01	27.83	28.59	26.09	28.51	25.66	27.36	26.61	27.39	25.09	28.34	28.18	29.48	28.73	28.46	30.37
Cr_2O_3	0.00	0.00	0.00	0.00	0.01	0.00	0.01	0.00	0.04	0.05	0.00	0.00	0.00	0.00	0.00	0.00	0.00	0.00	0.00
FeO^{total}	0.06	0.04	0.13	0.06	0.12	0.04	0.07	0.12	0.00	0.22	0.03	0.09	0.09	0.01	0.10	0.02	0.11	0.04	0.08
MnO	0.01	0.00	0.02	0.00	0.02	0.00	0.01	0.02	0.00	0.01	0.01	0.00	0.01	0.00	0.01	0.01	0.00	0.02	0.00
MgO	0.00	0.00	0.09	0.00	0.04	0.01	0.01	0.00	0.02	0.10	0.00	0.01	0.00	0.00	0.02	0.02	0.00	0.00	0.02
CaO	0.02	0.02	3.95	5.38	7.90	10.13	7.15	10.12	7.23	6.83	7.89	9.43	6.81	10.26	9.86	11.22	10.35	10.76	12.87
Na_2O	11.84	11.85	8.10	8.75	5.98	5.70	7.39	5.88	7.69	6.64	6.94	6.35	7.96	5.93	5.76	5.30	5.62	5.53	4.18
K_2O	0.04	0.04	1.52	0.02	0.92	0.07	0.08	0.09	0.06	1.16	0.12	0.01	0.01	0.04	0.36	0.04	0.10	0.04	0.11
Total	99.96	99.62	99.20	99.95	98.75	100.22	100.84	100.07	99.49	99.63	100.01	100.02	99.91	100.32	99.91	100.61	99.83	99.91	100.13
Oxygen#	8	8	8	8	8	8	8	8	8	8	8	8	8	8	8	8	8	8	8
Si	3.005	3.002	2.712	2.740	2.541	2.497	2.651	2.489	2.638	2.576	2.608	2.546	2.674	2.500	2.506	2.445	2.478	2.483	2.377
Ti	0.000	0.000	0.001	0.000	0.000	0.000	0.000	0.001	0.000	0.000	0.000	0.000	0.000	0.000	0.000	0.000	0.000	0.000	0.000
$Al^{(IV)}$	0.989	0.991	1.317	1.255	1.489	1.510	1.357	1.511	1.356	1.450	1.399	1.448	1.318	1.497	1.495	1.557	1.526	1.511	1.619
$Al^{(VI)}$	0.000	0.000	0.000	0.000	0.000	0.000	0.000	0.000	0.000	0.000	0.000	0.000	0.000	0.000	0.000	0.000	0.000	0.000	0.000
Cr	0.000	0.000	0.000	0.000	0.000	0.000	0.000	0.000	0.000	0.000	0.000	0.000	0.000	0.000	0.000	0.000	0.000	0.000	0.000
Fe^{3+}	0.002	0.002	0.005	0.002	0.005	0.002	0.003	0.005	0.000	0.008	0.001	0.004	0.003	0.000	0.004	0.001	0.004	0.002	0.003
Fe^{2+}	0.000	0.000	0.000	0.000	0.000	0.000	0.000	0.000	0.000	0.000	0.000	0.000	0.000	0.000	0.000	0.000	0.000	0.000	0.000
Mn	0.000	0.000	0.001	0.000	0.001	0.000	0.000	0.001	0.000	0.000	0.000	0.000	0.000	0.000	0.001	0.000	0.000	0.001	0.000
Mg	0.000	0.000	0.006	0.000	0.003	0.001	0.001	0.000	0.001	0.007	0.000	0.001	0.000	0.000	0.001	0.001	0.000	0.000	0.001
Ca	0.001	0.001	0.190	0.256	0.385	0.487	0.338	0.488	0.348	0.329	0.377	0.454	0.325	0.493	0.476	0.539	0.500	0.520	0.624
Na	1.003	1.008	0.705	0.753	0.527	0.496	0.633	0.513	0.669	0.579	0.601	0.552	0.689	0.515	0.503	0.461	0.492	0.483	0.366
K	0.002	0.002	0.087	0.001	0.053	0.004	0.005	0.005	0.003	0.067	0.007	0.000	0.000	0.002	0.021	0.002	0.006	0.002	0.006
Sum	5.002	5.006	5.024	5.007	5.004	4.997	4.988	5.013	5.015	5.016	4.993	5.005	5.009	5.007	5.007	5.006	5.006	5.002	4.996
Ab	99.70	99.70	71.80	74.60	54.60	50.30	64.90	51.00	65.60	59.40	61.00	54.90	67.90	51.00	50.30	46.00	49.30	48.10	36.70
An	0.10	0.10	19.30	25.30	39.90	49.30	34.60	48.50	34.10	33.70	38.30	45.10	32.10	48.80	47.60	53.80	50.10	51.70	62.70
Or	0.20	0.20	8.90	0.10	5.50	0.40	0.50	0.50	0.30	6.90	0.70	0.00	0.00	0.20	2.10	0.20	0.60	0.20	0.60

Table 1. ...Continued

Rock type	Contact zone between the metagabbros and hydrothermal veins														
Sample no.	751	751	757	757	757	754	751	754	754	754	754	751	751	754	754
Point no.	274	279	219	235	241	252	23	257	266	570	571	25-1	267	259	260
Mineral	Ab	Ab	Ab	Ab	Ab	Ab	Olig	Olig	Olig	Olig	Olig	Ande	Ande	Ano	Ano
SiO_2	69.25	69.29	68.29	68.52	66.24	68.95	62.11	62.62	62.57	60.46	61.54	59.50	59.53	64.22	62.57
TiO_2	0.00	0.01	0.00	0.00	0.00	0.00	0.00	0.01	0.00	0.00	0.00	0.02	0.00	0.00	0.00
Al_2O_3	19.35	19.56	19.68	19.72	21.05	19.46	23.78	22.62	23.85	24.02	23.63	25.25	25.83	23.35	24.34
Cr_2O_3	0.01	0.00	0.00	0.02	0.00	0.00	0.00	0.00	0.00	0.00	0.03	0.00	0.00	0.00	0.00
FeOtotal	0.00	0.00	0.04	0.01	0.13	0.12	0.13	1.03	0.04	0.10	0.09	0.08	0.01	0.23	0.13
MnO	0.02	0.00	0.01	0.00	0.00	0.01	0.03	0.03	0.01	0.00	0.00	0.00	0.00	0.00	0.01
MgO	0.01	0.00	0.00	0.00	0.05	0.01	0.01	1.37	0.00	0.01	0.03	0.00	0.01	0.11	0.26
CaO	0.02	0.24	0.59	0.66	1.73	0.37	5.16	2.82	5.48	5.20	5.09	6.73	7.70	1.10	1.17
Na_2O	10.84	10.93	10.84	10.84	10.00	10.94	9.09	8.49	7.99	8.06	8.75	7.69	6.93	8.17	7.74
K_2O	0.01	0.02	0.07	0.05	0.17	0.04	0.03	0.45	0.05	0.10	0.03	0.00	0.03	2.27	2.95
Total	99.49	100.04	99.52	99.82	99.37	99.88	100.33	99.43	99.99	97.94	99.19	99.26	100.03	99.46	99.15
Oxygen#	8	8	8	8	8	8	8	8	8	8	8	8	8	8	8
Si	3.023	3.012	2.992	2.992	2.919	3.007	2.749	2.787	2.765	2.734	2.751	2.668	2.650	2.844	2.792
Ti	0.000	0.000	0.000	0.000	0.000	0.000	0.000	0.000	0.000	0.000	0.000	0.001	0.000	0.000	0.000
Al(IV)	0.995	1.001	1.015	1.014	1.093	0.999	1.239	1.186	1.241	1.279	1.244	1.334	1.354	1.218	1.279
Al(VI)	0.000	0.000	0.000	0.000	0.000	0.000	0.000	0.000	0.000	0.000	0.000	0.000	0.000	0.000	0.000
Cr	0.000	0.000	0.000	0.000	0.000	0.000	0.000	0.000	0.000	0.000	0.000	0.000	0.000	0.000	0.000
Fe^{3+}	0.000	0.000	0.002	0.000	0.005	0.004	0.005	0.038	0.002	0.004	0.003	0.003	0.000	0.009	0.005
Fe^{2+}	0.000	0.000	0.000	0.000	0.000	0.000	0.000	0.000	0.000	0.000	0.000	0.000	0.000	0.000	0.000
Mn	0.001	0.000	0.000	0.000	0.000	0.000	0.001	0.001	0.000	0.000	0.000	0.000	0.000	0.000	0.000
Mg	0.000	0.000	0.000	0.000	0.003	0.000	0.001	0.091	0.000	0.000	0.002	0.000	0.001	0.007	0.017
Ca	0.001	0.011	0.028	0.031	0.082	0.017	0.245	0.134	0.260	0.252	0.244	0.323	0.367	0.052	0.056
Na	0.917	0.921	0.921	0.918	0.855	0.925	0.780	0.733	0.685	0.706	0.758	0.669	0.598	0.702	0.669
K	0.001	0.001	0.004	0.003	0.009	0.002	0.002	0.025	0.003	0.006	0.002	0.000	0.001	0.128	0.168
Sum	4.938	4.946	4.962	4.958	4.966	4.954	5.022	4.995	4.956	4.981	5.004	4.998	4.971	4.960	4.986
Ab	99.80	98.70	96.60	96.40	90.40	98.00	75.90	82.20	72.30	73.20	75.50	67.40	61.90	79.60	74.90
An	0.10	1.20	2.90	3.30	8.70	1.80	23.90	15.00	27.40	26.10	24.30	32.60	38.00	5.90	6.30
Or	0.10	0.10	0.50	0.30	0.90	0.20	0.20	2.80	0.30	0.70	0.20	0.00	0.10	14.50	18.80

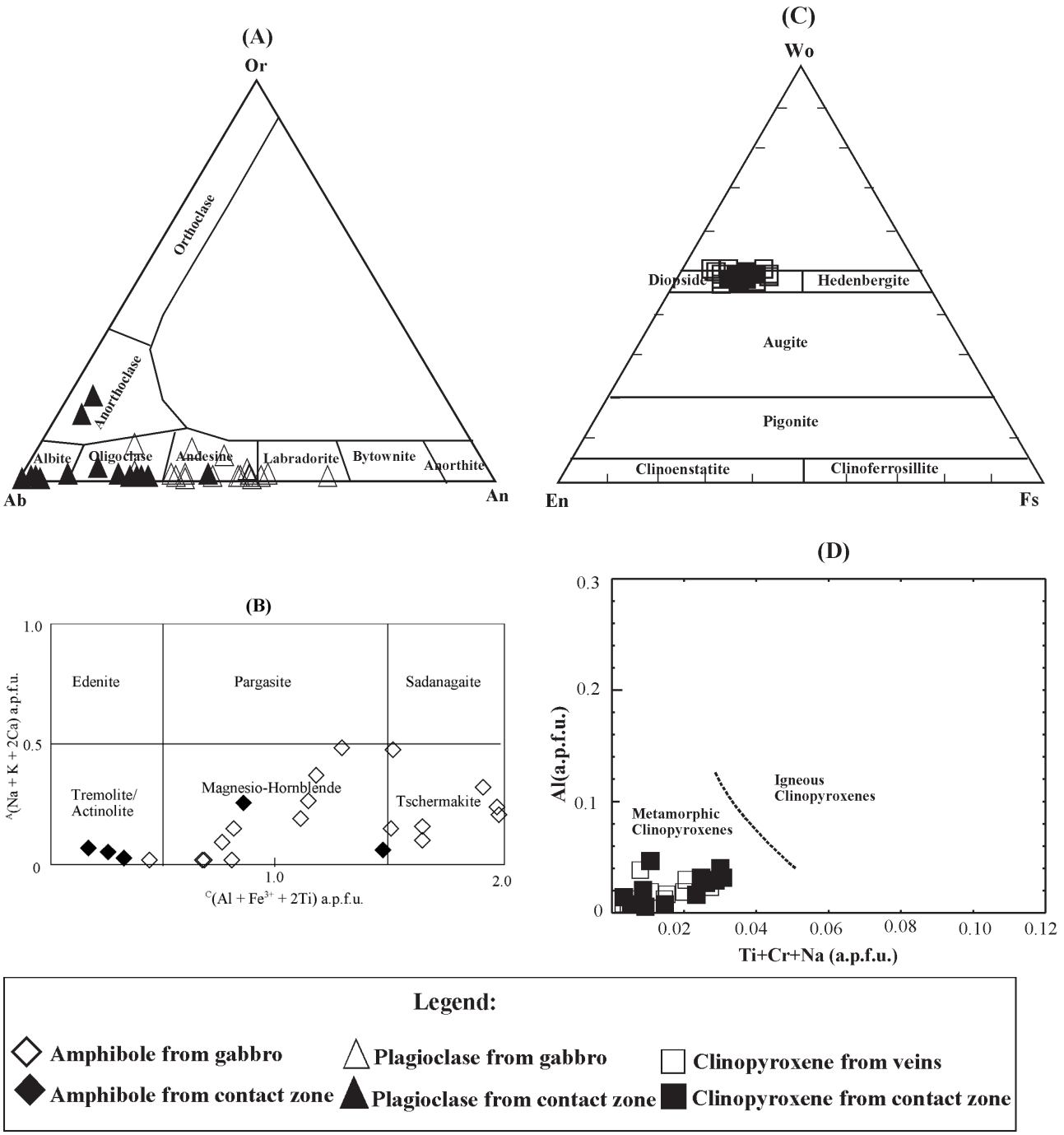

Figure 5. Mineral chemistry diagrams of the Jandaq ophiolite metagabbros and hydrothermal veins; (A) Feldspar classification triangle (Deer et al., 1992). (B) Amphibole classification graph (Hawthorne et al., 2012). (C) Pyroxene classification triangle (Morimoto, 1989). (D) The igneous and metamorphic clinopyroxene discrimination plot. The compositional gap between igneous and metamorphic pyroxene has been defined by Berger et al. (2005).

tschermakite, magnesio-hornblende and actinolite in the metagabbros (Figure 5B; Hawthorne et al., 2012) with Mg# 53.66 to 69.98, 60.81 to 89.04, and 60.81 to 88.36, respectively (Table 2). Low values of magnesio-hornblende (Mg# =67.90-80.93), and actinolite (Mg# = 82.02-91.18) are present in the contact zone (Table 2, Figure 5B).

The chemical analyses of minor minerals in the Jandaq

Table 2. Representative chemical compositions of amphiboles (in wt%) from the Jandaq ophiolite metagabbros and the contact zone (between the metagabbros and hydrothermal veins) and their calculated structural formula.

Rock type	Metagabbro										
Sample no.	624	624	624	640	763	763	763	760	760	760	760
Point no.	24	26	28	50	193	197	200	192	190	187	188
Mineral	Ts	Ts	Ts	Ts	Ts	Ts	Ts	Mg-Hbl	Mg-Hbl	Mg-Hbl	Mg-Hbl
SiO_2	42.79	42.56	41.62	41.53	45.33	45.55	45.19	50.84	44.82	48.44	46.94
TiO_2	0.54	0.58	0.41	0.66	1.16	0.89	0.72	0.34	0.08	0.38	0.44
Al_2O_3	15.85	15.33	16.42	14.04	12.12	12.15	12.67	6.63	13.18	9.25	10.82
Cr_2O_3	0.00	0.00	0.03	0.01	0.02	0.00	0.00	0.00	0.00	0.03	0.02
FeO^{total}	16.54	16.70	16.56	18.80	15.13	15.23	15.11	9.94	11.68	10.09	10.55
MnO	0.38	0.41	0.37	0.48	0.28	0.34	0.33	0.26	0.26	0.28	0.26
MgO	9.30	9.48	8.71	8.34	11.22	11.08	10.88	16.60	13.60	16.21	15.05
CaO	10.48	10.57	10.76	11.12	10.88	10.82	11.17	11.92	11.57	11.59	11.80
Na_2O	1.86	1.69	1.93	1.67	1.38	1.32	1.23	1.25	2.49	1.81	1.94
K_2O	0.39	0.40	0.42	1.10	0.37	0.36	0.40	0.04	0.11	0.08	0.10
Total	98.13	97.73	97.23	97.76	97.93	97.73	97.69	97.82	97.82	98.17	97.95
Oxygen#	23	23	23	23	23	23	23	23	23	23	23
Si	6.189	6.182	6.118	6.196	6.539	6.575	6.543	7.171	6.427	6.809	6.669
$Al^{(IV)}$	1.811	1.818	1.882	1.804	1.461	1.425	1.457	0.829	1.573	1.191	1.331
∑T	8.000	8.000	8.000	8.000	8.000	8.000	8.000	8.000	8.000	8.000	8.000
$Al^{(VI)}$	0.889	0.805	0.961	0.663	0.599	0.639	0.704	0.271	0.653	0.341	0.480
Ti	0.059	0.063	0.045	0.074	0.126	0.096	0.078	0.036	0.009	0.040	0.046
Cr	0.000	0.000	0.003	0.001	0.003	0.000	0.000	0.000	0.000	0.003	0.002
Fe^{2+}	1.038	0.982	1.227	1.602	1.035	1.027	1.119	0.635	0.766	0.418	0.644
Fe^{3+}	0.963	1.046	0.809	0.743	0.790	0.811	0.711	0.537	0.634	0.768	0.610
Mn	0.047	0.050	0.046	0.061	0.035	0.041	0.040	0.031	0.031	0.033	0.031
Mg	2.005	2.053	1.909	1.855	2.413	2.385	2.348	3.490	2.907	3.397	3.187
∑C	5.000	5.000	5.000	5.000	5.000	5.000	5.000	5.000	5.000	5.000	5.000
Ca	1.624	1.645	1.695	1.778	1.682	1.673	1.733	1.801	1.777	1.745	1.797
Na	0.376	0.355	0.305	0.222	0.318	0.327	0.267	0.199	0.223	0.255	0.203
∑B	2.000	2.000	2.000	2.000	2.000	2.000	2.000	2.000	2.000	2.000	2.000
Na	0.146	0.121	0.245	0.261	0.068	0.043	0.078	0.142	0.470	0.239	0.332
K	0.072	0.074	0.079	0.209	0.068	0.067	0.074	0.006	0.020	0.014	0.018
∑A	0.218	0.195	0.324	0.470	0.136	0.110	0.153	0.148	0.490	0.254	0.350
Sum	15.218	15.195	15.324	15.470	15.136	15.110	15.153	15.148	15.490	15.254	15.350
Fe#	34.11	32.36	39.13	46.34	30.02	30.10	32.28	15.39	20.85	10.96	16.81
Mg#	65.89	67.64	60.87	53.66	69.98	69.90	67.72	84.61	79.15	89.04	83.19

metagabbros indicate that chlorites are pycnochlorite in composition (Hey, 1954) with average Mg# of 65.18 and almost present in the margins of the altered amphiboles (Table 3). The opaque minerals are ilmenite, with the average TiO_2 and FeO^{total} amounts of 52.85 and 43.52 (wt%), respectively (Table 3). Biotites have FeO^{total}, TiO_2 and MgO values of 15.93 to 16.43, 1.59 to 1.71 and 12.55 to 12.77 (wt%), respectively (Table 3). The analyzed muscovites contain high values of Al_2O_3 (average 31.54 wt%) and low amounts of MgO (average 1.69 wt%) (Table 3).

Clinopyroxene and garnet occur as anhedral to subhedral

Table 2. ...Continued

Rock type	Metagabbro						Contact zone between the metagabbros and hydrothermal veins					
Sample no.	763	628	633	760	760	699	751	624-1	751	751	751	757
Point no.	205	30	32	183	181	213	24	60	22	25	268	236
Mineral	Mg-Hbl	Mg-Hbl	Mg-Hbl	Mg-Hbl	Mg-Hbl	Act	Mg-Hbl	Mg-Hbl	Act	Act	Act	Act
SiO_2	46.75	51.07	52.03	53.49	54.00	55.02	49.44	46.70	54.90	54.74	55.70	57.16
TiO_2	0.56	0.47	0.19	0.10	0.17	0.08	0.51	1.38	0.10	0.08	0.15	0.03
Al_2O_3	10.46	5.44	7.00	4.33	3.85	1.41	7.49	9.45	1.63	1.82	1.68	1.12
Cr_2O_3	0.00	0.10	0.08	0.00	0.00	0.00	0.06	0.00	0.01	0.04	0.08	0.00
FeO^{total}	15.48	11.70	7.16	8.45	8.34	11.11	10.69	16.95	7.84	7.13	8.80	6.08
MnO	0.26	0.29	0.23	0.24	0.25	0.24	0.22	0.49	0.08	0.20	0.23	0.25
MgO	10.87	15.68	17.41	18.24	18.37	17.12	15.97	11.16	18.70	19.58	18.40	20.64
CaO	11.75	12.09	12.15	12.25	12.09	12.08	12.42	10.62	12.80	12.91	12.46	12.73
Na_2O	0.91	0.71	0.68	0.71	0.70	0.35	1.23	1.19	0.44	0.38	0.40	0.19
K_2O	0.46	0.38	0.06	0.03	0.03	0.02	0.10	0.49	0.01	0.05	0.04	0.04
Total	97.50	97.96	97.00	97.85	97.80	97.44	98.17	98.43	96.58	96.94	97.95	98.24
Oxygen#	23	23	23	23	23	23	23	23	23	23	23	23
Si	6.840	7.271	7.303	7.467	7.529	7.796	7.014	6.739	7.807	7.710	7.799	7.858
$Al^{(IV)}$	1.160	0.729	0.697	0.533	0.471	0.204	0.986	1.261	0.193	0.290	0.201	0.142
∑T	8.000	8.000	8.000	8.000	8.000	8.000	8.000	8.000	8.000	8.000	8.000	8.000
$Al^{(VI)}$	0.642	0.183	0.460	0.178	0.161	0.030	0.266	0.344	0.081	0.012	0.076	0.039
Ti	0.062	0.050	0.020	0.011	0.018	0.008	0.054	0.150	0.011	0.009	0.016	0.003
Cr	0.000	0.011	0.009	0.000	0.000	0.000	0.007	0.000	0.001	0.005	0.009	0.000
Fe^{2+}	1.528	0.911	0.503	0.517	0.503	0.927	0.796	1.135	0.869	0.595	0.800	0.409
Fe^{3+}	0.366	0.482	0.337	0.469	0.469	0.389	0.472	0.911	0.064	0.245	0.231	0.290
Mn	0.032	0.035	0.027	0.028	0.030	0.029	0.026	0.060	0.009	0.024	0.028	0.029
Mg	2.371	3.328	3.643	3.796	3.819	3.616	3.378	2.401	3.965	4.111	3.841	4.230
∑C	5.000	5.000	5.000	5.000	5.000	5.000	5.000	5.000	5.000	5.000	5.000	5.000
Ca	1.843	1.844	1.827	1.833	1.806	1.834	1.888	1.642	1.951	1.949	1.870	1.875
Na	0.157	0.156	0.173	0.167	0.189	0.097	0.112	0.333	0.049	0.051	0.108	0.051
∑B	2.000	2.000	2.000	2.000	1.994	1.931	2.000	1.975	2.000	2.000	1.977	1.926
Na	0.101	0.040	0.012	0.026	0.000	0.000	0.226	0.000	0.073	0.053	0.000	0.000
K	0.086	0.069	0.011	0.005	0.005	0.004	0.018	0.090	0.001	0.009	0.006	0.007
∑A	0.187	0.109	0.023	0.031	0.005	0.004	0.244	0.090	0.074	0.062	0.006	0.007
Sum	15.187	15.109	15.023	15.031	14.999	14.934	15.244	15.065	15.074	15.062	14.984	14.932
Fe#	39.19	21.49	12.13	11.99	11.64	20.41	19.07	32.10	17.98	12.64	17.24	8.82
Mg#	60.81	78.51	87.87	88.01	88.36	79.59	80.93	67.90	82.02	87.36	82.76	91.18

crystals along the veins wall and in inner part of the veins. Clinopyroxenes are diopside in compositions (Figure 5C; Morimoto, 1989). Chemistry of clinopyroxenes in the contact zone shows Mg# = 73.66-89.79, Cr_2O_3<0.04 (wt%), TiO_2<0.81 (wt%) and Al_2O_3 values of 0.25-1.12 (wt%) (Table 4). Clinopyroxenes from the inner part of the veins have lower values of Mg# (78.21-80.60), Cr_2O_3 (bdl), TiO_2 (<0.05 wt%) and Al_2O_3 (<0.94 wt%) (Table 4). Chemical compositions of the clinopyroxenes, as well as using the Al versus Ti+Cr+Na diagram, indicate their metamorphic nature (Figure 5D; Berger et al., 2005). The ACF chemographic diagram (Figure 6) shows the position of the all analyzed hydrothermal minerals from the studied veins (Figure 6).

The coarse grained-garnets with porphyroblastic texture are present as a major mineral in the inner part of the veins

Table 3. Representative chemical compositions of chlorite, mica and opaque minerals (in wt%) from the Jandaq ophiolite metagabbros and their calculated structural formula.

Rock type			Metagabbro												
Sample no.	699	Sample no.	763	763	763	760	760	760	757	757	Sample no.	760	760	763	763
Point no.	211	Point no.	195	199	202	185	186	189	230	231	Point no.	177	178	196	204
Mineral	Pych	Mineral	Bt	Bt	Bt	Ms	Ms	Ms	Ms	Ms	Mineral	Ilm	Ilm	Ilm	Ilm
SiO_2	28.25	SiO_2	37.49	37.56	37.63	52.00	49.14	49.93	46.94	46.78	SiO_2	0.01	0.00	0.00	0.01
TiO_2	0.01	TiO_2	1.71	1.59	1.59	0.00	0.01	0.00	0.00	0.00	TiO_2	52.72	52.63	52.83	53.25
Al_2O_3	20.09	Al_2O_3	17.57	17.52	17.91	30.22	32.17	32.23	35.70	34.98	Al_2O_3	0.00	0.00	0.00	0.01
Cr_2O_3	0.00	Cr_2O_3	0.00	0.00	0.00	0.03	0.00	0.00	0.00	0.00	Cr_2O_3	0.03	0.00	0.00	0.00
FeO^{total}	19.35	FeO^{total}	16.43	15.93	16.43	0.60	0.61	0.68	0.25	0.36	FeO^{total}	44.41	44.47	43.26	41.94
MnO	0.17	MnO	0.14	0.17	0.14	0.00	0.02	0.03	0.00	0.00	MnO	2.12	2.23	3.51	4.13
MgO	20.58	MgO	12.77	12.71	12.55	1.87	2.40	0.81	0.35	0.97	MgO	0.54	0.47	0.15	0.12
CaO	0.00	CaO	0.04	0.05	0.01	0.34	0.08	0.58	0.05	0.02	CaO	0.00	0.00	0.00	0.00
Na_2O	0.00	Na_2O	0.10	0.15	0.12	1.77	0.13	2.28	0.38	0.16	Na_2O	0.04	0.00	0.03	0.01
K_2O	0.00	K_2O	9.16	9.32	9.05	9.05	11.17	8.22	11.03	11.09	K_2O	0.00	0.00	0.00	0.00
Total	88.43	Total	95.41	94.99	95.42	95.88	95.72	94.75	94.69	94.36	Sum	99.86	99.80	99.78	99.46
Oxygen#	28	Oxygen#	22	22	22	11	11	11	11	11	Oxygen#	3	3	3	3
Si	5.689	Si	5.592	5.620	5.602	3.392	3.244	3.294	3.126	3.130	Si	0.000	0.000	0.000	0.000
Ti	0.001	Ti	0.192	0.179	0.177	0.000	0.000	0.000	0.000	0.000	Ti	0.999	0.997	1.004	1.016
$Al^{(IV)}$	2.311	$Al^{(IV)}$	2.408	2.380	2.398	2.322	2.501	2.504	2.799	2.756	$Al^{(IV)}$	0.000	0.000	0.000	0.000
$Al^{(VI)}$	2.454	$Al^{(VI)}$	0.678	0.706	0.743	0.000	0.000	0.000	0.000	0.000	$Al^{(VI)}$	0.000	0.000	0.000	0.000
Cr	0.000	Cr	0.000	0.000	0.000	0.002	0.000	0.000	0.000	0.000	Cr	0.000	0.000	0.000	0.000
Fe^{3+}	0.000	Fe^{3+}	0.000	0.000	0.000	0.000	0.000	0.000	0.000	0.000	Fe^{3+}	0.006	0.005	0.002	0.004
Fe^{2+}	3.259	Fe^{2+}	2.049	1.993	2.046	0.033	0.033	0.038	0.014	0.020	Fe^{2+}	0.928	0.932	0.912	0.887
Mn	0.028	Mn	0.017	0.022	0.017	0.000	0.001	0.001	0.000	0.000	Mn	0.045	0.048	0.075	0.089
Mg	6.178	Mg	2.839	2.835	2.785	0.182	0.236	0.080	0.034	0.097	Mg	0.020	0.018	0.006	0.004
Ca	0.000	Ca	0.007	0.007	0.002	0.024	0.006	0.041	0.004	0.002	Ca	0.000	0.000	0.000	0.000
Na	0.000	Na	0.029	0.042	0.034	0.224	0.016	0.292	0.049	0.020	Na	0.002	0.002	0.001	0.000
K	0.001	K	1.743	1.779	1.718	0.753	0.941	0.692	0.937	0.947	K	0.000	0.000	0.000	0.000
Sum	19.921	Sum	15.554	15.563	15.522	6.932	6.978	6.942	6.963	6.972	Sum	2.000	2.000	2.000	2.000
Fe#	0.35	Fe#	0.42	0.41	0.42	0.15	0.12	0.32	0.29	0.17					
Mg#	0.65	Mg#	0.58	0.59	0.58	0.85	0.88	0.68	0.71	0.83					

Table 4. Representative chemical compositions of clinopyroxene (in wt%) from the contact zone (between the metagabbros and hydrothermal veins) and the hydrothermal veins and their calculated structural formula.

Rock type	Contact zone between the metagabbros and hydrothermal veins																
Sample no.	751	751	751	754	754	754	754	754	754	754	754	757	757	757	757	757	757
Point no.	21	26	27	256	258	262	263	264	265	572	574	224	226	228	229	233	237
Mineral	Di	Di	Di	Di	Di	Di	Di	Di	Di	Di	Di	Di	Di	Di	Di	Di	Di
SiO_2	53.54	54.07	53.30	54.25	53.95	53.51	53.15	53.55	53.40	52.81	51.86	53.42	53.46	54.16	54.12	53.54	54.00
TiO_2	0.04	0.00	0.00	0.05	0.03	0.00	0.04	0.07	0.06	0.09	0.05	0.21	0.00	0.03	0.15	0.81	0.07
Al_2O_3	0.74	0.77	0.31	0.39	0.41	0.44	0.73	0.72	0.65	0.80	0.52	1.12	0.25	0.36	0.94	0.91	0.57
Cr_2O_3	0.00	0.00	0.00	0.00	0.00	0.00	0.00	0.02	0.00	0.02	0.04	0.03	0.00	0.00	0.04	0.00	0.01
FeO^{total}	6.93	6.99	6.92	6.86	6.91	8.47	9.50	7.80	7.83	7.84	8.00	4.34	7.25	5.58	3.27	4.11	5.76
MnO	0.17	0.11	0.22	0.22	0.18	0.22	0.22	0.23	0.19	0.18	0.26	0.25	0.55	0.37	0.18	0.26	0.19
MgO	14.65	15.22	14.61	14.41	14.37	13.29	11.98	13.61	13.41	13.44	13.31	15.56	13.47	14.57	16.12	15.33	15.62
CaO	23.65	24.37	24.48	23.75	23.67	23.78	23.62	23.51	23.46	23.63	23.63	24.83	24.67	25.13	25.13	25.08	23.46
Na_2O	0.36	0.40	0.14	0.22	0.27	0.22	0.36	0.33	0.31	0.37	0.27	0.11	0.08	0.02	0.07	0.07	0.14
K_2O	0.00	0.00	0.02	0.00	0.01	0.00	0.00	0.00	0.00	0.02	0.00	0.00	0.00	0.00	0.00	0.00	0.01
Total	100.07	101.90	100.00	100.14	99.79	99.93	99.60	99.84	99.30	99.19	97.94	99.86	99.73	100.21	100.03	100.10	99.82
Oxygen#	8	8	8	8	8	8	8	8	8	8	8	8	8	8	8	8	8
Si	1.978	1.958	1.975	2.009	2.003	2.000	2.005	1.996	2.003	1.981	1.973	1.964	1.999	2.001	1.979	1.970	1.992
Ti	0.001	0.000	0.000	0.001	0.001	0.000	0.001	0.002	0.002	0.002	0.002	0.006	0.000	0.001	0.004	0.022	0.002
$Al^{(IV)}$	0.022	0.033	0.014	0.000	0.000	0.000	0.000	0.004	0.000	0.019	0.023	0.036	0.001	0.000	0.022	0.030	0.008
$Al^{(VI)}$	0.010	0.000	0.000	0.017	0.018	0.019	0.032	0.028	0.029	0.016	0.000	0.013	0.010	0.016	0.019	0.009	0.017
Cr	0.000	0.000	0.000	0.000	0.000	0.000	0.000	0.001	0.000	0.001	0.001	0.001	0.000	0.000	0.001	0.000	0.000
Fe^{3+}	0.035	0.080	0.048	0.000	0.000	0.000	0.000	0.000	0.000	0.025	0.047	0.018	0.000	0.000	0.000	0.000	0.000
Fe^{2+}	0.180	0.132	0.167	0.213	0.215	0.265	0.300	0.243	0.246	0.220	0.209	0.116	0.227	0.172	0.100	0.126	0.178
Mg	0.807	0.821	0.807	0.795	0.796	0.741	0.673	0.756	0.750	0.751	0.755	0.853	0.751	0.802	0.879	0.841	0.859
Mn	0.005	0.003	0.007	0.007	0.006	0.007	0.007	0.007	0.006	0.006	0.008	0.008	0.017	0.012	0.006	0.008	0.006
Ca	0.936	0.945	0.972	0.942	0.942	0.952	0.955	0.939	0.943	0.949	0.963	0.978	0.989	0.995	0.985	0.989	0.927
Na	0.026	0.028	0.010	0.016	0.019	0.016	0.027	0.024	0.023	0.027	0.020	0.008	0.006	0.001	0.005	0.005	0.010
K	0.000	0.000	0.001	0.000	0.000	0.000	0.000	0.000	0.000	0.001	0.000	0.000	0.000	0.000	0.000	0.000	0.001
Sum	4.000	4.000	4.001	4.000	4.000	4.000	4.000	4.000	4.002	3.998	4.001	4.001	4.000	4.000	4.000	4.000	4.000
Fe#	0.18	0.14	0.17	0.21	0.21	0.26	0.31	0.24	0.25	0.23	0.22	0.12	0.23	0.18	0.10	0.13	0.17
Mg#	0.82	0.86	0.83	0.79	0.79	0.74	0.69	0.76	0.75	0.77	0.78	0.88	0.77	0.82	0.90	0.87	0.83

Table 4. ...Continued

Rock type	Hydrothermal veins									
Sample no.	751-1	751-1	751-1	751	751	751	751	751	753	753
Point no.	169	170	172	270	271	272	280	281	242	243
Mineral	Di	Di	Di	Di	Di	Di	Di	Di	Di	Di
SiO_2	53.85	53.77	53.94	53.76	54.05	54.05	54.10	54.09	53.89	53.38
TiO_2	0.03	0.01	0.00	0.05	0.03	0.05	0.00	0.00	0.02	0.00
Al_2O_3	0.51	0.48	0.42	0.73	0.29	0.62	0.19	0.17	0.33	0.94
Cr_2O_3	0.00	0.00	0.00	0.00	0.00	0.01	0.00	0.00	0.00	0.00
FeO^{total}	6.87	6.63	6.47	6.64	6.25	6.44	6.63	6.04	6.90	6.94
MnO	0.21	0.22	0.22	0.27	0.25	0.19	0.24	0.25	0.23	0.19
MgO	13.87	14.02	14.27	14.33	14.54	14.35	14.43	14.69	14.09	13.66
CaO	24.43	24.43	24.41	23.95	24.01	23.78	24.06	24.22	24.15	24.33
Na_2O	0.21	0.26	0.22	0.28	0.17	0.34	0.14	0.08	0.24	0.20
K_2O	0.00	0.00	0.00	0.01	0.00	0.00	0.00	0.00	0.00	0.00
Total	99.97	99.82	99.94	100.01	99.59	99.82	99.79	99.53	99.85	99.65
Oxygen#	8	8	8	8	8	8	8	8	8	8
Si	2.001	1.998	2.000	1.991	2.009	2.004	2.010	2.012	2.003	1.990
Ti	0.001	0.000	0.000	0.001	0.001	0.001	0.000	0.000	0.001	0.000
$Al^{(IV)}$	0.000	0.002	0.000	0.009	0.000	0.000	0.000	0.000	0.000	0.010
$Al^{(VI)}$	0.022	0.019	0.018	0.023	0.013	0.027	0.008	0.007	0.014	0.032
Cr	0.000	0.000	0.000	0.000	0.000	0.000	0.000	0.000	0.000	0.000
Fe^{3+}	0.000	0.001	0.000	0.003	0.000	0.000	0.000	0.000	0.000	0.000
Fe^{2+}	0.214	0.205	0.201	0.203	0.194	0.199	0.206	0.188	0.215	0.217
Mg	0.768	0.777	0.788	0.791	0.806	0.793	0.800	0.814	0.781	0.759
Mn	0.007	0.007	0.007	0.009	0.008	0.006	0.007	0.008	0.007	0.006
Ca	0.972	0.972	0.970	0.950	0.956	0.945	0.958	0.965	0.962	0.972
Na	0.015	0.019	0.015	0.020	0.012	0.025	0.010	0.006	0.017	0.014
K	0.000	0.000	0.000	0.000	0.000	0.000	0.000	0.000	0.000	0.000
Sum	4.000	4.000	3.999	4.000	3.999	4.000	3.999	4.000	4.000	4.000
Fe#	0.22	0.21	0.20	0.20	0.19	0.20	0.20	0.19	0.22	0.22
Mg#	0.78	0.79	0.80	0.80	0.81	0.80	0.80	0.81	0.78	0.78

(Figure 4 G,H). The average values of CaO, Al_2O_3, and FeO^{total} of garnets from the contact zone are 34.99, 18.10 and 6.80 (wt%), respectively. The values of these elements in the garnets from the inner part of the veins are 35.86, 18.80 and 5.37 (wt%), respectively (Table 5). The garnets are grossular-andradite in the composition ($Grs_{67-94}Adr_{2-25}$ in the veins margin and $Grs_{76-91}Adr_{6-20}$ in the core of veins).

Calcite is the main mineral in the veins with average CaO value of 59.44 wt% (Table 6). Prehnite with a nearly homogeneous chemistry is commonly present in the margin and core of the veins. They are Fe-poor with average CaO and Al_2O_3 values of 27.23 and 24.32 wt%, respectively (Table 7, Figure 6). The analyzed epidotes from the margin of the veins present PS# values [$100*Fe^{3+}/(Al^{VI}+Fe^{3+})$] of 16.21 to 27.30 (Table 8).

Trace elements

Clinopyroxenes have low amounts of Al, Ti, Cr, Mn, Na, K and REE possibly support their non-magmatic nature (Table 4, 9). They have higher values of the LREE in the margin of veins. Garnets in the studied veins present great heterogeneity with lower LREE and higher HREE amounts in the margin compared to the inner part of the veins (Figure 7A, Table 9). Clinopyroxenes and garnets from the contact zone have higher values of REEs

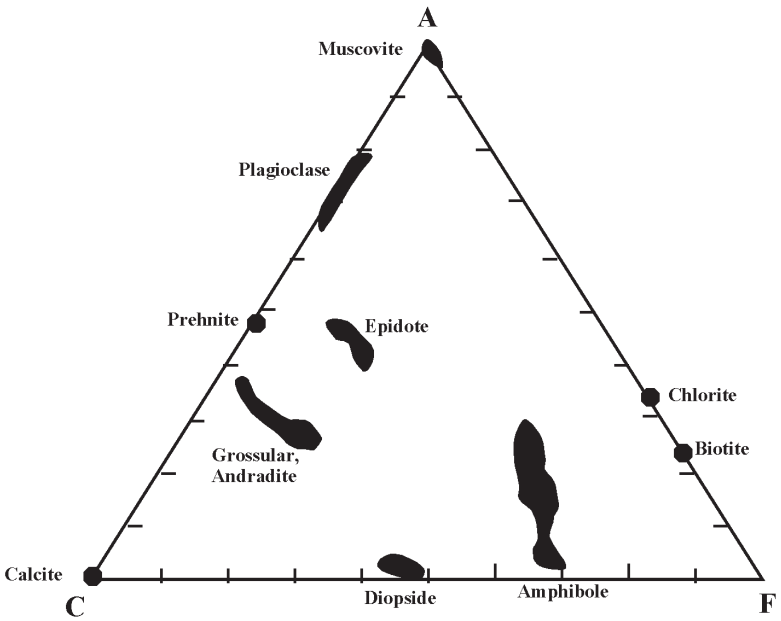

Figure 6. ACF ternary chemical diagram and position of the rock- forming minerals of the Jandaq hydrothermal veins and enclosing metagabbros.

relative to the core of the veins (Figure 7A). Epidote and prehnite have very low values of REEs, as well as positive anomaly of Eu in the chondrite- normalized REE patterns (Fig 7A).

Amphiboles of the metagabbros present high values of REE and negative anomaly of Eu (Figure 7B), support their magmatic nature. On the other hand, amphiboles in the contact zones have lower REE contents and show positive anomaly of Eu (Figure 7B). Plagioclases of the metagabbros show a significant positive anomaly of Eu in the chondrite- normalized REE patterns (Figure 7B).

The primitive mantle-normalized multi-element spidergram of the magmatic amphiboles from the metagabbros (Figure 7D) show negative anomalies of Rb, Th, La, Sr, Zr, Hf and Ti (normalization factors after McDonough and Sun, 1995). The plagioclases present negative anomalies of Ce, Pr and Zr and positive spikes of Pb, Sr and Eu in this diagram (Figure 7D).

DISCUSSION

Discrimination of magmatic and hydrothermal amphiboles

Petrographic characteristics, major and trace elements chemical compositions and geothermometry results of the amphiboles are useful to determine their magmatic or hydrothermal origin (e.g., Gillis and Meyer, 2001 and references therein). According to the petrographic studies, three types of amphiboles are present in the investigated metagabbros and the associated veins:

(1) Granular amphiboles in the metagabbros are brown to greenish brown in color and are associated with plagioclase and ilmenite (Figure 4 A,B). These igneous amphiboles are tschermakite and magnesio-hornblende in composition (Table 2).

(2) Amphiboles commonly occur as rim around the clinopyroxenes in the contact zone between metagabbros and hydrothermal veins. These types of amphiboles are actinolite in composition (Table 2, Figure 5B).

(3) Brown to green amphiboles that completely or partially enclose the clinopyroxene grains (Figure 4D), are classified as magnesio-hornblende and actinolite (Table 2, Figure 5B). These types of amphiboles have fine inclusions of magnetite.

The low amounts of Al^{VI} and high values of Al^{IV} in the calculated structural formula of the studied amphiboles in the metagabbros (Table 2), indicate high occupancy of the tetrahedral site by aluminum (more than 90% of Al). The amounts of FeO^{total} are high (7.16-18.80 wt%), most of them are characterized by low amounts of Fe^{3+} and high contents of Fe^{2+} (Table 2). The chemical compositions of amphiboles in the studied metagabbros indicate they are calcic, silica and magnesia poor, ferroan rich and have most of their aluminum in the tetrahedral site (Figure 6). The contents of Al^{total} and (Na+K) vary from 0.1 to 2.8 (a.p.f.u.) and 0.1 to 0.7 (a.p.f.u.), respectively (Figure 8). No significant changes are observed in the Ti values in the chemical compositions of amphiboles from the metagabbros. The mineral chemistry of the studied three types of amphiboles shows that granular amphiboles in

Table 5. Representative chemical compositions of garnet (in wt%) from the contact zone (between the metagabbros and hydrothermal veins) and the hydrothermal veins and their calculated structural formula.

Rock type		Contact zone between metagabbros and hydrothermal veins												
Sample no.		751	751	751	754	754	757	757	757	757	757	754	754	751
Point no.		20	275	278	578	580	217	222	223	239	240	253	254	273
Mineral		Grt	Grt	Grt	Grt	Grt	Grt	Grt	Grt	Grt	Grt	Grt	Grt	Grt
SiO_2		39.16	39.81	39.92	39.33	38.33	39.67	39.84	40.19	40.03	39.19	39.18	39.46	39.53
TiO_2		0.00	0.03	0.03	0.05	0.10	0.05	0.00	0.03	0.23	0.42	0.13	0.13	0.05
Al_2O_3		19.30	18.38	20.51	18.08	16.29	19.86	20.77	21.57	21.18	16.14	16.47	16.50	17.04
Cr_2O_3		0.00	0.00	0.00	0.01	0.00	0.00	0.00	0.00	0.00	0.00	0.00	0.01	0.00
FeO^{total}		5.03	5.80	3.40	6.01	10.92	4.18	2.77	1.53	1.74	8.73	9.84	9.93	9.02
MnO		0.09	0.07	0.10	0.07	0.09	0.13	0.19	0.15	0.20	0.74	0.11	0.10	0.08
MgO		0.07	0.02	0.06	0.11	0.10	0.08	0.11	0.50	0.41	0.21	0.06	0.09	0.05
CaO		36.19	35.86	35.79	35.25	33.03	35.77	36.05	36.08	36.26	34.26	34.19	33.83	34.13
Na_2O		0.00	0.00	0.01	0.03	0.00	0.00	0.00	0.01	0.00	0.00	0.00	0.00	0.00
K_2O		0.00	0.00	0.00	0.00	0.01	0.00	0.00	0.00	0.00	0.00	0.00	0.00	0.00
Total		99.84	99.96	99.82	98.93	98.87	99.74	99.73	100.06	100.04	99.68	99.96	100.06	99.91
Oxygen#		12	12	12	12	12	12	12	12	12	12	12	12	12
Si		2.982	3.038	3.028	3.033	2.996	3.018	3.019	3.021	3.015	3.031	3.023	3.042	3.044
Ti		0.000	0.002	0.002	0.003	0.006	0.003	0.000	0.001	0.013	0.024	0.008	0.008	0.003
$Al^{(IV)}$		0.018	0.000	0.000	0.000	0.004	0.000	0.000	0.000	0.000	0.000	0.000	0.000	0.000
$Al^{(VI)}$		1.713	1.652	1.832	1.642	1.496	1.779	1.854	1.910	1.878	1.470	1.496	1.498	1.546
Cr		0.000	0.000	0.000	0.000	0.000	0.000	0.000	0.000	0.000	0.000	0.000	0.001	0.000
Fe^{3+}		0.299	0.264	0.104	0.286	0.491	0.172	0.103	0.042	0.060	0.415	0.439	0.398	0.356
Fe^{2+}		0.021	0.106	0.112	0.102	0.223	0.094	0.073	0.054	0.049	0.149	0.196	0.242	0.225
Mn		0.005	0.005	0.006	0.005	0.006	0.008	0.012	0.009	0.013	0.048	0.007	0.007	0.005
Mg		0.008	0.002	0.007	0.013	0.012	0.009	0.013	0.056	0.046	0.024	0.006	0.011	0.005
Ca		2.953	2.932	2.909	2.912	2.766	2.916	2.927	2.905	2.926	2.838	2.826	2.794	2.816
Na		0.000	0.000	0.001	0.004	0.000	0.000	0.000	0.002	0.000	0.000	0.000	0.000	0.000
K		0.000	0.000	0.000	0.000	0.000	0.000	0.000	0.000	0.000	0.000	0.000	0.000	0.000
Sum		7.999	8.001	8.001	8.000	8.000	7.999	8.001	8.000	8.000	7.999	8.001	8.001	8.000
Fe#		0.72	0.98	0.94	0.89	0.95	0.91	0.85	0.49	0.52	0.86	0.97	0.96	0.98
Mg#		0.28	0.02	0.06	0.11	0.05	0.09	0.15	0.51	0.48	0.14	0.03	0.04	0.02
End Members	Alm	0.716	3.479	3.690	3.348	7.410	3.091	2.409	1.791	1.627	4.880	6.459	7.939	7.376
	Adr	14.860	13.789	5.358	14.794	24.646	8.819	5.262	2.152	3.074	21.758	22.582	20.883	18.695
	Grs	83.983	82.513	90.501	81.104	67.354	87.507	91.522	93.841	93.384	71.010	70.524	70.565	73.588
	Prp	0.258	0.071	0.224	0.428	0.391	0.307	0.415	1.851	1.503	0.772	0.208	0.346	0.177
	Sps	0.184	0.149	0.203	0.159	0.198	0.275	0.393	0.311	0.412	1.580	0.226	0.222	0.165
	Uv	0.000	0.000	0.000	0.019	0.000	0.000	0.000	0.000	0.000	0.000	0.000	0.045	0.000

Table 5. ...Continued

Rock type		Hydrothermal veins					
Sample no.		751-1	751-1	751-1	751-1	753	753
Point no.		158	161	163	174	244	247
Mineral		Grt	Grt	Grt	Grt	Grt	Grt
SiO_2		39.67	39.41	40.00	39.64	39.36	40.02
TiO_2		0.03	0.03	0.10	0.04	0.03	0.05
Al_2O_3		18.32	17.28	20.36	18.68	18.08	20.08
Cr_2O_3		0.00	0.00	0.00	0.00	0.00	0.00
FeO^{total}		6.10	7.56	3.19	5.76	6.17	3.49
MnO		0.08	0.04	0.06	0.06	0.07	0.11
MgO		0.05	0.05	0.08	0.07	0.06	0.06
CaO		35.70	35.70	36.28	35.64	35.79	36.07
Na_2O		0.00	0.02	0.00	0.00	0.00	0.01
K_2O		0.01	0.00	0.00	0.00	0.00	0.00
Total		99.95	100.09	100.07	99.88	99.57	99.88
Oxygen#		12	12	12	12	12	12
Si		3.029	3.017	3.026	3.025	3.018	3.036
Ti		0.002	0.002	0.005	0.002	0.002	0.003
$Al^{(IV)}$		0.000	0.000	0.000	0.000	0.000	0.000
$Al^{(VI)}$		1.647	1.558	1.814	1.679	1.632	1.794
Cr		0.000	0.000	0.000	0.000	0.000	0.000
Fe^{3+}		0.286	0.402	0.118	0.261	0.323	0.125
Fe^{2+}		0.103	0.082	0.083	0.107	0.073	0.097
Mn		0.005	0.003	0.004	0.004	0.005	0.007
Mg		0.006	0.005	0.009	0.007	0.007	0.007
Ca		2.921	2.929	2.941	2.915	2.940	2.931
Na		0.000	0.003	0.000	0.000	0.000	0.001
K		0.000	0.000	0.000	0.000	0.000	0.000
Sum		7.999	8.001	8.000	8.000	8.000	8.001
Fe#		0.94	0.94	0.90	0.94	0.91	0.93
Mg#		0.06	0.06	0.10	0.06	0.09	0.07
End Members	Alm	3.407	2.709	2.742	3.524	2.407	3.186
	Adr	14.777	20.501	6.104	13.430	16.489	6.481
	Grs	81.436	76.441	90.732	82.683	80.717	89.841
	Prp	0.188	0.178	0.297	0.244	0.234	0.230
	Sps	0.175	0.088	0.124	0.119	0.152	0.232
	Uv	0.012	0.000	0.000	0.000	0.000	0.000

the metagabbros are rich in Al, Ti, and (Na+K) (Figure 8 A,B). Some amphibole and plagioclase crystals in the studied metagabbros exhibit chemical variations possibly can be attributed to the hydrothermal alteration effects.

Estimation of temperatures provides useful information about the origin of the amphiboles. Equilibrium temperatures were calculated for plagioclase-amphibole pairs using the edenite + albite = richterite + anorthite exchange geothermometer (Holland and Blundy, 1994). The average values of the calculated temperatures

Table 6. Representative chemical compositions of calcite (in wt%) from the hydrothermal veins and the contact zone (between the metagabbros and hydrothermal veins) and their calculated structural formula.

Rock type	Hydrothermal veins							Contact zone between the metagabbros and hydrothermal veins		
Sample no.	751-1	751-1	751-1	751-1	753	753	753	757	757	757
Point no.	159	166	167	175	248	249	250	218	220	221
Mineral	Cal	Cal	Cal	Cal	Cal	Cal	Cal	Cal	Cal	Cal
SiO_2	0.00	0.00	0.00	0.00	0.14	0.00	0.00	0.02	0.00	0.00
TiO_2	0.00	0.00	0.00	0.00	0.00	0.00	0.00	0.00	0.01	0.03
Al_2O_3	0.01	0.00	0.00	0.01	0.02	0.00	0.01	0.00	0.00	0.01
Cr_2O_3	0.00	0.00	0.00	0.00	0.00	0.00	0.00	0.00	0.00	0.00
FeO^{total}	0.04	0.00	0.01	0.00	0.05	0.04	0.00	0.01	0.03	0.07
MnO	0.04	0.00	0.00	0.03	0.01	0.02	0.01	0.01	0.10	0.05
MgO	0.01	0.01	0.01	0.00	0.02	0.00	0.01	0.00	0.11	0.04
CaO	61.11	60.41	61.55	61.12	60.18	60.15	58.75	52.77	57.36	61.02
Na_2O	0.00	0.00	0.00	0.00	0.02	0.01	0.00	0.00	0.00	0.00
K_2O	0.00	0.00	0.00	0.00	0.00	0.00	0.00	0.01	0.00	0.00
Total	61.20	60.42	61.56	61.17	60.45	60.21	58.78	52.82	57.62	61.22
Oxygen#	3	3	3	3	3	3	3	3	3	3
Si	0.000	0.000	0.000	0.000	0.007	0.000	0.000	0.001	0.000	0.000
Ti	0.000	0.000	0.000	0.000	0.000	0.000	0.000	0.000	0.000	0.001
$Al^{(IV)}$	0.000	0.000	0.000	0.000	0.001	0.000	0.000	0.000	0.000	0.000
$Al^{(VI)}$	0.000	0.000	0.000	0.000	0.000	0.000	0.000	0.000	0.000	0.000
Cr	0.000	0.000	0.000	0.000	0.000	0.000	0.000	0.000	0.000	0.000
Fe^{3+}	0.000	0.000	0.000	0.000	0.000	0.000	0.000	0.000	0.000	0.000
Fe^{2+}	0.001	0.001	0.000	0.000	0.003	0.001	0.000	0.000	0.001	0.001
Mn	0.001	0.001	0.000	0.001	0.001	0.001	0.001	0.001	0.004	0.002
Mg	0.000	0.000	0.000	0.002	0.001	0.000	0.000	0.000	0.008	0.003
Ca	2.998	2.998	3.000	2.997	2.985	2.998	2.999	2.998	2.987	2.993
Na	0.000	0.000	0.000	0.000	0.002	0.000	0.000	0.000	0.000	0.000
K	0.000	0.000	0.000	0.000	0.000	0.000	0.000	0.000	0.000	0.000
Sum	3.000	3.000	3.000	3.000	3.000	3.000	3.000	3.000	3.000	3.000

by amphibole-plagioclase geothermometry are 706 and 524 ºC for the metagabbros and the contact zone, respectively. Thermometry of the igneous amphiboles in the metagabbros using the "Ti-content of amphibole" thermometry (Otten, 1984) suggest 616º to 698 ºC for their formation. Most of the granular amphiboles in the metagabbros equilibrated at higher temperatures than hydrothermal amphiboles in the contact zone. Based on the Al-in-amphibole geobarometry (Schmidt, 1992); P (±0.6kbar)=4.76Al^{total}-3.01, the igneous amphiboles yield pressure ranges of 5.56 to 9.84 kbar. Calculation of the fO_2 values using the Wons (1989) equation; Log fO_2=-30930/T+14.98+0.142(P-1)/T for the Jandaq metagabbros, show ranges of -15.90 to -19.46. In these calculations, temperature and pressure of the magmatic amphiboles are considered as 616º to 698 ºC and 5.56 to 9.84 kbar, respectively. These ranges of the fO_2 indicate high values of the fO_2 and oxidation state of the environment.

Trace elements chemical compositions of amphiboles are useful for discrimination of the magmatic and hydrothermal amphiboles. REE contents of the amphiboles in metagabbros indicate LREE enrichment relative to the HREE with $[Ce/Yb]_{CN}$=1.27-2.12. They have ratios of $[Ce/Sm]_{CN}$<1, $[Dy/Er]_{CN}$~1.2, and $[Eu/Eu^*]_{CN}$=0.59-0.66. But amphiboles in the contact zones

Table 7. Representative chemical compositions of prehnite (in wt%) from the hydrothermal veins and the contact zone (between the metagabbros and hydrothermal veins) and their calculated structural formula.

Rock type	Hydrothermal veins							Contact zone between the metagabbros and hydrothermal veins				
Sample no.	751-1	751-1	751-1	751-1	751-1	751-1	751-1	757	757	757	757	757
Point no.	160	162	164	165	168	171	176	225	232	238	245	246
Mineral	Prh	Prh	Prh	Prh	Prh	Prh	Prh	Prh	Prh	Prh	Prh	Prh
SiO_2	44.10	44.29	44.25	44.48	44.46	44.11	44.30	43.94	44.07	44.60	44.01	44.11
TiO_2	0.00	0.00	0.00	0.00	0.00	0.00	0.01	0.00	0.00	0.00	0.00	0.00
Al_2O_3	24.21	24.48	24.24	24.28	24.37	24.56	24.12	24.14	23.82	23.09	24.15	24.31
Cr_2O_3	0.00	0.00	0.00	0.00	0.00	0.00	0.00	0.00	0.00	0.00	0.00	0.00
FeO^{total}	0.31	0.18	0.13	0.08	0.33	0.04	0.39	0.09	0.04	0.44	0.00	0.02
MnO	0.00	0.00	0.00	0.00	0.00	0.02	0.00	0.00	0.01	0.03	0.01	0.03
MgO	0.00	0.00	0.00	0.00	0.00	0.00	0.00	0.02	0.00	1.15	0.01	0.00
CaO	27.38	27.13	27.20	27.18	27.42	27.04	27.24	26.84	26.05	24.74	27.10	26.98
Na_2O	0.02	0.01	0.00	0.00	0.01	0.00	0.00	0.06	0.14	0.16	0.00	0.01
K_2O	0.01	0.00	0.00	0.00	0.01	0.01	0.00	0.00	0.13	0.42	0.00	0.00
Total	96.03	96.10	95.81	96.01	96.59	95.78	96.07	95.10	94.26	94.63	95.29	95.46
Oxygen#	22	22	22	22	22	22	22	22	22	22	22	22
Si	6.041	6.048	6.061	6.075	6.050	6.040	6.062	6.061	6.120	6.169	6.060	6.059
Ti	0.000	0.000	0.000	0.000	0.000	0.000	0.001	0.000	0.000	0.000	0.000	0.000
$Al^{(IV)}$	3.908	3.941	3.914	3.909	3.909	3.964	3.889	3.924	3.899	3.764	3.919	3.935
$Al^{(VI)}$	0.000	0.000	0.000	0.000	0.000	0.000	0.000	0.000	0.000	0.000	0.000	0.000
Cr	0.000	0.000	0.000	0.000	0.000	0.000	0.000	0.000	0.000	0.000	0.000	0.000
Fe^{3+}	0.000	0.000	0.000	0.000	0.000	0.000	0.000	0.000	0.000	0.000	0.000	0.000
Fe^{2+}	0.035	0.021	0.015	0.009	0.037	0.005	0.044	0.011	0.005	0.051	0.000	0.002
Mn	0.000	0.000	0.000	0.000	0.000	0.003	0.000	0.000	0.001	0.004	0.001	0.003
Mg	0.000	0.000	0.000	0.000	0.000	0.000	0.000	0.003	0.001	0.237	0.002	0.000
Ca	4.018	3.970	3.992	3.997	3.998	3.967	3.994	3.968	3.876	3.666	3.998	3.972
Na	0.006	0.002	0.000	0.000	0.003	0.000	0.001	0.015	0.038	0.043	0.000	0.003
K	0.002	0.001	0.000	0.000	0.002	0.001	0.000	0.001	0.022	0.075	0.000	0.000
Sum	14.010	13.983	13.982	13.990	13.999	13.980	13.991	13.983	13.962	14.009	13.980	13.974

have lower REE contents compared to the amphiboles in metagabbros with $[Ce/Yb]_{CN}$=0.75-1.42. The studied amphiboles from the contact zone present ratios of $[Ce/Sm]_{CN}$>1, $[Dy/Er]_{CN}$~0.9, and $[Eu/Eu^*]_{CN}$=1.29-3.36. Chondrite-normalized REE patterns of the amphiboles and clinopyroxenes from the contact zone indicate that the amphiboles are slightly more enriched in REE than the clinopyroxenes (Figure 7B). Correlations between the major and trace elements chemical compositions and textures of the amphiboles indicate that the granular amphiboles in the metagabbros have a general decrease in $[Dy]_{CN}$ (46.43-61.46) and increase in $[Eu/Eu^*]_{CN}$ (0.58-0.66) with an increase in $Al^{(total)}$ (1.80-2.06) (Table 9). Whereas, the acicular amphibole rims around the clinopyroxenes and amphibole pseudomorphs after clinopyroxene exhibit high-$Al^{(total)}$ (0.63-2.22), low-$[Dy]_{CN}$ (3.46-8.18) and high-$[Eu/Eu^*]_{CN}$ (1.29-3.36) grains from the contact zone.

Using the $[Ce]_{CN}$ versus $[Dy]_{CN}$ graph shows that the granular amphiboles in the metagabbros follow the gabbro crystallization trend (Figure 9). This trend possibly indicates their magmatic nature. Amphibole grains in the contact zone follow a general mixing trend between clinopyroxene and plagioclase (Figure 9). This trend possibly suggests that their REE contents are affected by local mineral-scale reactions involving clinopyroxene,

Table 8. Representative chemical compositions of epidote (in wt%) from the hydrothermal veins and the contact zone (between the metagabbros and hydrothermal veins) and their calculated structural formula.

Rock type	Hydrothermal veins						Contact zone between the metagabbros and hydrothermal veins					
Sample no.	751	751	754	754	754	754	640	640	699	699	699	699
Point no.	276	277	251	261	573	577	48	52	207	208	210	212
Mineral	Ep	Ep	Ep	Ep	Ep	Ep	Ep	Ep	Ep	Ep	Ep	Ep
SiO_2	38.72	38.92	39.00	39.05	37.12	39.12	38.36	38.65	38.38	38.50	38.46	38.30
TiO_2	0.23	0.24	0.06	0.03	0.01	0.23	0.12	0.10	0.03	0.01	0.07	0.03
Al_2O_3	24.26	24.29	26.33	27.07	24.32	20.81	24.98	25.27	23.31	23.31	23.65	23.39
Cr_2O_3	0.00	0.00	0.01	0.00	0.00	0.02	0.00	0.00	0.04	0.01	0.00	0.00
FeO^{total}	10.54	10.36	8.94	7.36	10.17	10.95	10.54	9.71	11.85	12.11	11.71	11.99
MnO	0.04	0.03	0.09	0.08	0.04	0.15	0.26	0.22	0.12	0.12	0.10	0.09
MgO	0.04	0.02	0.02	0.06	0.04	0.11	0.05	0.15	0.00	0.01	0.00	0.04
CaO	23.32	23.38	22.87	23.48	22.62	26.29	22.49	22.34	23.39	23.41	23.47	23.33
Na_2O	0.00	0.00	0.01	0.00	0.02	0.05	0.02	0.00	0.02	0.01	0.00	0.00
K_2O	0.01	0.00	0.00	0.00	0.02	0.00	0.01	0.02	0.00	0.00	0.00	0.01
Total	97.16	97.24	97.31	97.12	94.35	97.72	96.83	96.46	97.14	97.49	97.45	97.17
Oxygen#	12.5	12.5	12.5	12.5	12.5	12.5	12.5	12.5	12.5	12.5	12.5	12.5
Si	3.044	3.055	3.038	3.041	3.006	3.102	3.021	3.045	3.034	3.034	3.028	3.027
Ti	0.013	0.014	0.004	0.002	0.000	0.014	0.007	0.006	0.002	0.001	0.004	0.002
$Al^{(IV)}$	0.000	0.000	0.000	0.000	0.000	0.000	0.000	0.000	0.000	0.000	0.000	0.000
$Al^{(VI)}$	2.246	2.245	2.415	2.482	2.319	1.944	2.317	2.344	2.170	2.163	2.193	2.177
Cr	0.000	0.000	0.000	0.000	0.000	0.001	0.000	0.000	0.002	0.001	0.000	0.000
Fe^{3+}	0.690	0.680	0.580	0.480	0.690	0.730	0.690	0.640	0.780	0.800	0.770	0.790
Fe^{2+}	0.000	0.000	0.000	0.000	0.000	0.000	0.000	0.000	0.000	0.000	0.000	0.000
Mn	0.003	0.002	0.006	0.005	0.003	0.010	0.017	0.015	0.008	0.008	0.007	0.006
Mg	0.005	0.002	0.003	0.007	0.005	0.012	0.006	0.018	0.000	0.001	0.000	0.004
Ca	1.964	1.966	1.908	1.958	1.962	2.234	1.898	1.886	1.981	1.977	1.980	1.975
Na	0.000	0.000	0.001	0.000	0.003	0.007	0.003	0.000	0.003	0.001	0.000	0.000
K	0.001	0.000	0.000	0.000	0.002	0.000	0.001	0.002	0.000	0.000	0.000	0.001
Sum	7.966	7.964	7.955	7.975	7.990	8.054	7.960	7.956	7.980	7.986	7.982	7.982
Ps	0.235	0.232	0.194	0.162	0.229	0.273	0.229	0.214	0.264	0.270	0.260	0.266

plagioclase, and hydrothermal fluids. These amphiboles are possibly inherited the REE patterns of the primary clinopyroxenes (Figure 7B). But, enrichment in LREE and Eu relative to clinopyroxene and correlation of these REEs with Al values show the influence of plagioclase. Based on the trace elements chemical compositions of minerals in the metagabbros, during the crystallization of amphibole and plagioclase, the Pb, Sr and Eu prefer to enter in plagioclase structure more than the amphibole one (Figure 7D). Because, partition coefficient (Kd) of these elements in the plagioclase is higher than the amphibole (Blundy and Wood, 1994; Klein et al., 1997).

Amphibole is present as a minor phase in the water-rich magmas from the volcanic arcs (e.g., Rutherford et al., 1985; Sisson and Layne, 1993; Sato et al., 1999; Webster, 1992; Sisson and Grove, 1993; Gillis and Meyer, 2001 and references therein). Chemical analyses of the melt inclusions in the phenocrysts (Sisson and Layne, 1993) and the results of experimental investigations on amphibole stability (Rutherford et al., 1985; Sisson and Grove, 1993; Sato et al., 1999), indicate that the H_2O content of the magma saturated with amphibole is typically between 2 to 6 wt%. The H_2O-saturated magmas are typical of the subduction zone-related ones. But the

Table 9. Microprobe (major elements) and LA-ICP-MS (trace elements) analyses of minerals from the metagabbros, contact zones and hydrothermal veins of the Jandaq ophiolite.

Rock type	Metagabbros				Contact zone between the metagabbros and hydrothermal veins			
Sample no.	763				760			
Point no.	193	197	205	194	181	187	190	192
Mineral	Amp	Amp	Amp	Pl	Amp	Amp	Amp	Amp
SiO_2	45.33	45.55	46.75	55.73	53.99	48.44	44.82	50.84
TiO_2	1.16	0.89	0.56	0.00	0.17	0.38	0.08	0.34
Al_2O_3	12.12	12.14	10.46	28.34	3.85	9.25	13.18	6.63
FeO^{total}	15.13	15.23	15.48	0.01	8.34	10.09	11.68	9.94
MnO	0.28	0.34	0.26	0.00	0.25	0.28	0.26	0.26
MgO	11.22	11.08	10.87	0.00	18.37	16.21	13.60	16.60
CaO	10.88	10.82	11.75	10.26	12.09	11.58	11.57	11.92
Na_2O	1.38	1.32	0.91	5.93	0.70	1.81	2.49	1.25
K_2O	0.37	0.36	0.46	0.04	0.03	0.08	0.11	0.04
Total	97.93	97.73	97.50	100.32	97.80	98.17	97.82	97.82
Rb	2.609	1.826	2.034	16.079	0.129	0.150	0.118	0.087
Sr	39.473	37.610	34.297	1414.797	7.601	4.174	7.277	2.117
Y	79.438	70.155	59.620	0.303	12.372	5.795	7.998	5.144
Zr	61.410	37.058	27.352	0.014	6.496	3.579	3.712	7.493
Nb	7.788	6.337	5.535	0.000	0.998	1.136	0.407	0.445
Ba	124.404	59.425	15.936	141.811	1.080	1.590	1.404	0.781
La	5.141	4.912	10.993	1.883	0.989	1.393	0.882	0.782
Ce	42.766	36.208	51.285	2.490	3.919	4.107	3.631	2.571
Pr	9.260	7.672	8.728	0.220	0.629	0.537	0.522	0.341
Nd	52.528	45.053	45.124	0.783	3.161	2.238	2.467	1.466
Sm	15.069	13.718	12.206	0.077	0.951	0.553	0.647	0.407
Eu	2.858	2.803	2.541	0.455	0.475	0.639	0.678	0.301
Gd	14.660	13.325	11.434	0.092	1.311	0.608	0.842	0.575
Tb	2.242	2.004	1.725	0.007	0.250	0.104	0.155	0.114
Dy	15.119	13.430	11.423	0.032	2.013	0.853	1.182	0.875
Ho	3.009	2.693	2.282	0.003	0.434	0.187	0.291	0.187
Er	8.520	7.502	6.302	0.021	1.213	0.576	0.901	0.603
Tm	1.211	1.075	0.918	0.007	0.181	0.096	0.150	0.092
Yb	8.226	7.492	6.355	0.011	1.225	0.757	1.278	0.647
Lu	1.113	1.005	0.850	0.000	0.160	0.103	0.193	0.096
Hf	3.021	2.359	2.088	0.008	0.417	0.146	0.065	0.381
Ta	0.434	0.313	0.339	0.000	0.042	0.039	0.006	0.019
Pb	5.314	3.910	5.922	21.461	0.078	0.038	0.054	0.038
Th	0.071	0.080	0.449	0.003	0.043	0.010	0.066	0.157
U	0.083	0.142	0.171	0.005	0.011	0.009	0.007	0.021
$[Ce/Yb]_{CN}$	1.37	1.27	2.12	57.19	0.84	1.43	0.75	1.04
Eu/Eu*	0.59	0.63	0.66	16.44	1.30	3.36	2.80	1.90

Table 9. ...Continued

Rock type	Contact zone between the metagabbros and hydrothermal veins				Hydrothermal veins			
Sample no.	751-1				751			
Point no.	161	162	169	172	271	272	273	276
Mineral	Grt	Prh	Cpx	Cpx	Cpx	Cpx	Grt	Ep
SiO_2	39.41	44.29	53.84	53.94	54.05	54.04	39.53	38.72
TiO_2	0.03	0.00	0.03	0.00	0.03	0.05	0.05	0.23
Al_2O_3	17.28	24.48	0.51	0.42	0.29	0.62	17.04	24.26
FeO^{total}	7.56	0.18	6.87	6.47	6.25	6.44	9.02	10.54
MnO	0.04	0.00	0.21	0.22	0.25	0.19	0.08	0.04
MgO	0.05	0.00	13.90	14.26	14.54	14.35	0.05	0.04
CaO	35.70	27.13	24.43	24.41	24.01	23.78	34.13	23.32
Na_2O	0.02	0.01	0.21	0.21	0.17	0.34	0.00	0.00
K_2O	0.00	0.00	0.00	0.00	0.00	0.00	0.00	0.01
Total	100.09	96.10	100.00	99.98	99.61	99.82	99.91	97.16
Rb	0.002	0.019	0.006	0.030	0.003	0.003	0.003	0.003
Sr	1.505	1.198	10.777	9.332	15.622	15.515	1.501	0.387
Y	0.295	0.019	4.440	6.808	5.176	4.514	5.158	0.149
Zr	0.780	0.021	1.617	4.043	2.319	1.885	7.138	0.865
Nb	0.003	0.001	0.001	0.003	0.002	0.002	0.026	0.491
Ba	0.014	0.106	1.173	0.323	0.043	0.007	0.011	0.049
La	0.013	0.013	0.028	0.038	0.270	0.235	0.001	0.015
Ce	0.105	0.034	0.239	0.304	1.143	1.019	0.010	0.362
Pr	0.016	0.003	0.060	0.077	0.192	0.168	0.010	0.067
Nd	0.054	0.011	0.453	0.645	1.101	0.950	0.181	0.170
Sm	0.003	0.004	0.194	0.353	0.429	0.353	0.142	0.015
Eu	0.024	0.006	0.031	0.033	0.142	0.123	0.489	0.037
Gd	0.014	0.012	0.343	0.573	0.712	0.596	0.316	0.023
Tb	0.001	0.002	0.064	0.115	0.132	0.113	0.064	0.002
Dy	0.021	0.004	0.584	0.957	1.003	0.823	0.580	0.018
Ho	0.007	0.002	0.150	0.236	0.217	0.179	0.147	0.003
Er	0.030	0.000	0.478	0.750	0.586	0.518	0.469	0.009
Tm	0.008	0.002	0.071	0.112	0.086	0.081	0.070	0.002
Yb	0.074	0.001	0.537	0.789	0.601	0.558	0.545	0.017
Lu	0.013	0.000	0.097	0.117	0.111	0.101	0.075	0.002
Hf	0.001	0.000	0.066	0.235	0.099	0.079	0.143	0.016
Ta	0.002	0.000	0.000	0.004	0.000	0.000	0.000	0.001
Pb	0.061	0.306	0.079	0.081	0.263	0.100	0.008	0.029
Th	0.002	0.000	0.001	0.004	0.000	0.001	0.000	0.001
U	0.032	0.002	0.003	0.003	0.001	0.000	0.101	0.032
$[Ce/Yb]_{CN}$	0.37	11.21	0.12	0.10	0.50	0.48	0.01	5.44
Eu/Eu*	11.03	2.51	0.37	0.23	0.78	0.82	7.03	6.12

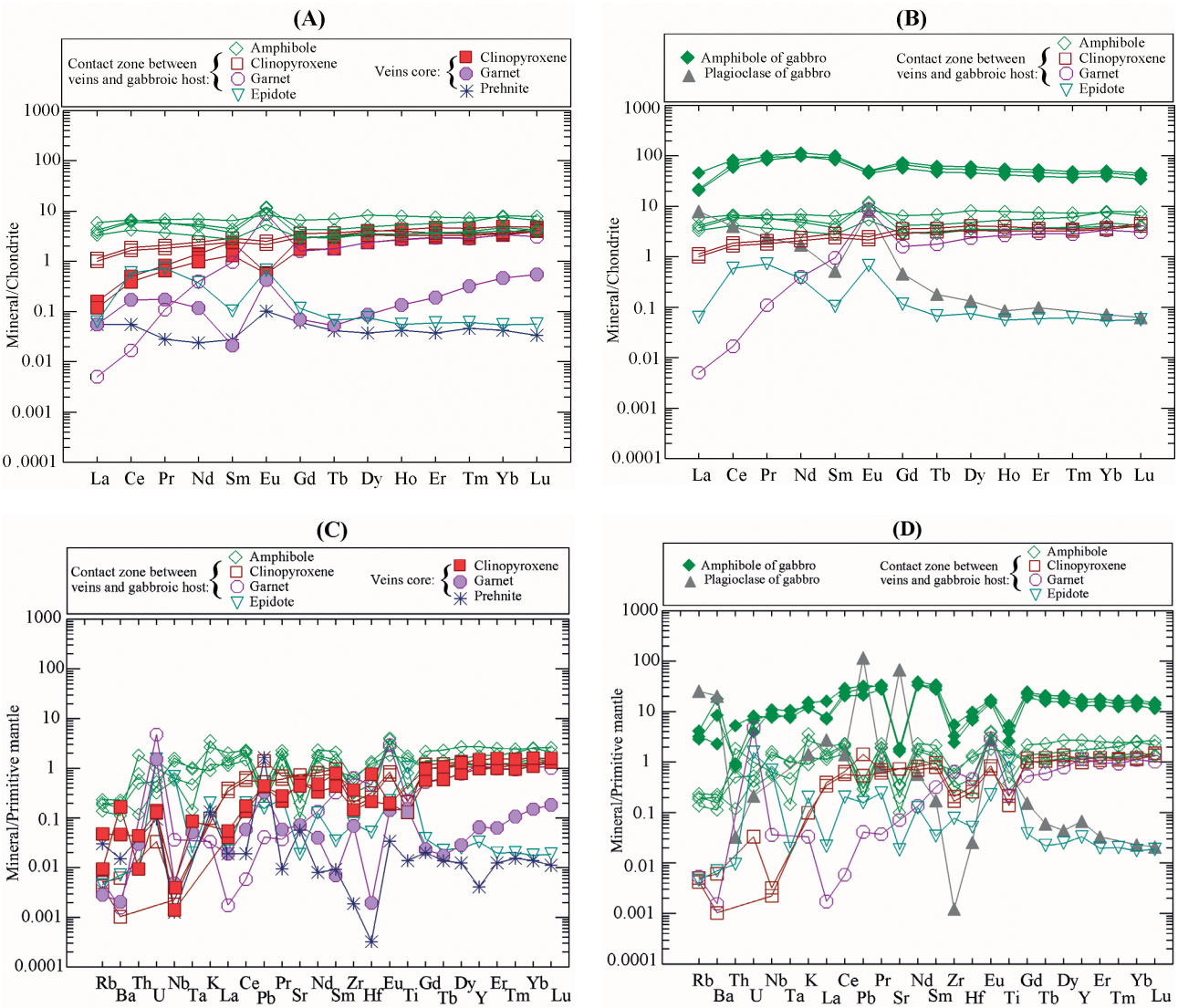

Figure 7. Chondrite-normalized REE patterns (A,B) and primitive mantle-normalized spidergram (C,D) of the minerals from the studied hydrothermal veins and enclosing metagabbros of the Jandaq ophiolite. Normalizing values of the chondrite and primitive mantle are taken from Sun and McDonough (1989), and McDonough and Sun (1995), respectively.

magmas of the mid-ocean ridges have low content of the H_2O. The N-MORB and E-MORB magmas which form the igneous amphiboles, have 0.1-0.2 wt% and up to 0.6 wt% H_2O, respectively (e.g., Sobolev and Chaussidon, 1996, Gillis and Meyer, 2001). Therefore, the granular amphiboles with magmatic origin in the metagabbros are formed by the melts enriched in H_2O. The geological and tectonic history of the CEIM confirm a supra-subduction zone setting (back-arc) for the ophiolitic mélange of Paleozoic age in the Yazd block (e.g., Bagheri, 2007; Bagheri and Stampfli, 2008; Torabi and Aria, 2013; Shafaii Moghadam and Stern, 2014; Nosouhian et al., 2016; Berra et al., 2017; Nosouhian et al., 2019).

Petrogenesis of the hydrothermal veins

The Joints and cracks of the Jandaq gabbroic intrusions are filled by hydrothermal minerals. Nicolas et al. (2003) propose that penetration of the seawater has been introduced along the grain boundaries and fractures in the deep oceanic crust. Rock-forming minerals of the studied contact zones consist of hydrous (amphibole + chlorite + epidote + prehnite) and anhydrous (plagioclase + clinopyroxene + garnet + albite) minerals. Most of the minerals are hydrous silicates. The high abundance of the hydrous minerals in the contact zone suggest that the fluid flow was focused along the joints and cracks with enhanced permeability.

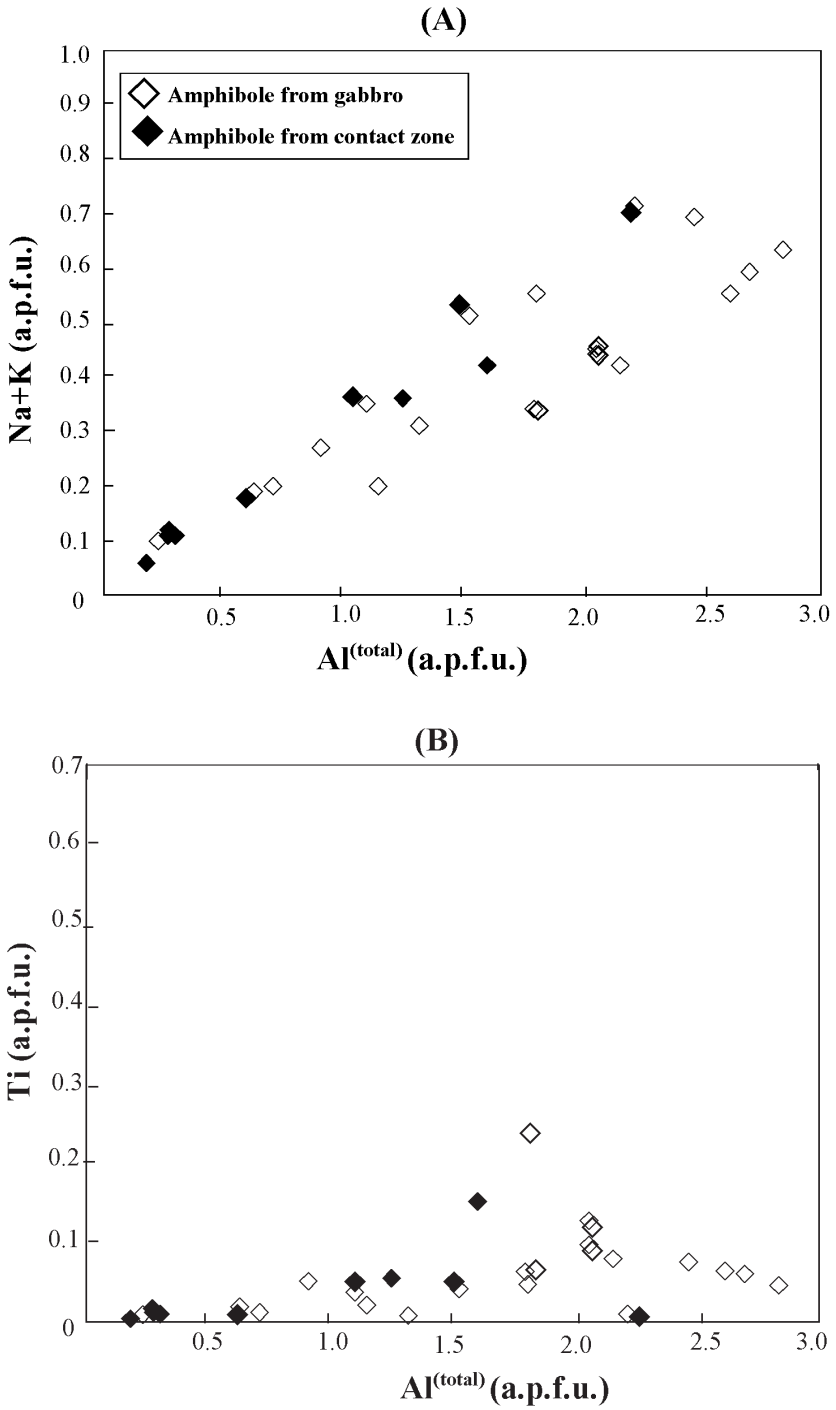

Figure 8. Major elements chemical compositions of the amphiboles in the metagabbros and contact zone between the metagabbros and hydrothermal veins; (A) Na + K versus $Al^{(total)}$ (B) Ti versus $Al^{(total)}$.

The temperature estimation of the metamorphism can be constrained roughly by mineralogical assemblage. In the NaO-CaO-FeO-MgO-Al_2O_3-SiO_2-H_2O system, varying amounts of sodic plagioclase + diopside + actinolite + prehnite + epidote can crystallize at temperatures between 300 and 450 ^oC (e.g., McCollom and Shock, 1998 and references therein; Bach et al., 2012). The stability range of the prehnite and epidote in the similar rocks is

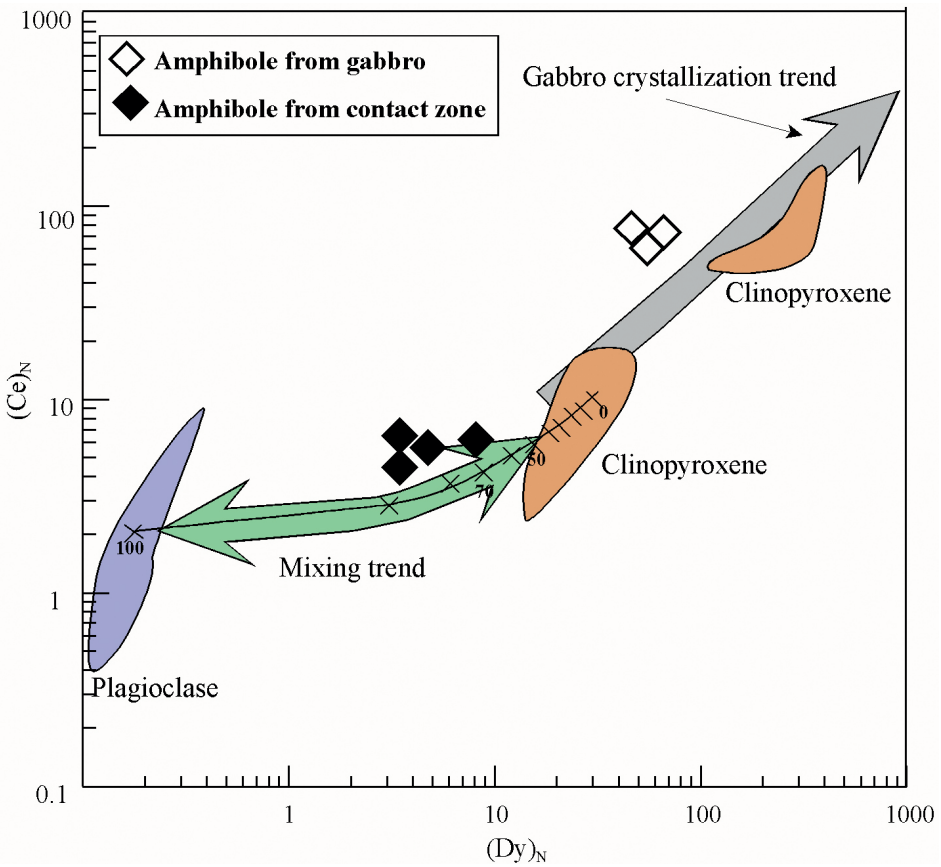

Figure 9. $[Ce]_{CN}$ versus $[Dy]_{CN}$ values of amphibole in the metagabbros and contact zone between the metagabbros and hydrothermal veins. The green arrow with a black line is a simple mixing trend between average plagioclase and clinopyroxene values; numbers indicate the percentage of plagioclase in the mix. The gray arrow shows the gabbro crystallization trend. The plagioclase and clinopyroxene fields are from (Gillis and Meyer, 2001 and references therein).

220-430 °C and >300 ºC, respectively (e.g., Liou et al., 1983; Bach et al., 2012). At 450 ºC, prehnite + epidote are no longer present among the equilibrium minerals, leaving alteration assemblage of plagioclase + diopside + actinolite. These three minerals are stable up to a temperature of 650 ºC (e.g., McCollom and Shock, 1998). Over this temperature, amphiboles are no longer present among the predicted equilibrium minerals, leaving an alteration assemblage of clinopyroxene and garnet (e.g., McCollom and Shock, 1998). The presence of diopside association with grossular-andradite suggests the high temperature ranging from 500 to 800 ºC (Frost et al., 2008). These petrological results reveal that the mineral assemblages of the hydrothermal veins from the Jandaq area are typical result of the interaction between the metagabbros and seawater-derived fluids (e.g., McCollom and Shock, 1998). The core of the hydrothermal veins and contact zones within the Jandaq metagabbros record the high, medium and low temperature hydrous alteration, ranging from 650-800 °C, 450-650 °C, and 300-450 °C, respectively. The core of veins mainly consists of high-temperature mineral association of calcite + clinopyroxene + garnet ± oxides. The modal values of the hydrous minerals increase with decreasing the temperature. Medium- temperature mineral assemblage in the contact zone is plagioclase (andesine, oligoclase) + clinopyroxene + amphibole (magnesio-hornblende, actinolite) + chlorite ± garnet ± oxides followed by low- temperature alteration paragenesis mainly consists of epidote + prehnite + actinolite. One of the most important characteristics of the studied veins is high abundance of calcite, which is an evidence for the high fCO_2 of the hydrothermal fluids. The chemical compositions of the minerals from the Jandaq hydrothermal veins and enclosing gabbros are plotted in the ACF (Al-Ca-(Fe+Mg)) ternary diagram (Figure 6). The higher CaO and MgO values, and the lower Al_2O_3 and FeO^{total} amounts in the metagabbros relative to the veins can be attributed to the metasomatism (Figure 6).

Such metasomatism is responsible for the hydrothermal processes active within the oceanic crust (e.g., Puga et al., 1999; Kitajima et al., 2001; Huot et al., 2002).

Minerals of the investigated veins exhibit wide ranges of the patterns in the chondrite-normalized REE diagram (Figure 7), indicates chemical heterogeneity of the hydrothermal fluids. LREE-enrichment cannot be achieved by a closed system crystallization. The REE mobility via aqueous fluids occurs at temperatures up to 700 °C (Lieftink et al., 1994). Activity of the REEs gradually decreases in the hydrothermal solutions by decreasing the temperature of the solution or the host. The REE-enriched diopsides and relatively REE-depleted garnets precipitated in the studied veins core by a high temperature hydrothermal solution (e.g., Python et al., 2007 a;b; Figure 7). The LREE and Eu have higher mobility in hydrothermal fluids involved in the studied veins (Figure 7 A,B). After downward ingression and circulation of the hydrothermal fluids through the crustal section, when reaching the mantle-crust transition zone, the hydrothermal fluids lose the alkalic elements by precipitation of minerals like amphibole, epidote, albite in the crustal hydrothermal veins. These minerals are selectively enriched in the elements like Ca and Eu due to their interaction with the gabbros from the lower crust. Therefore, the positive Eu anomaly of the hydrothermal minerals in the chondrite-normalized REE patterns associated with high modal amounts of calcite, and the presence of Ca-rich minerals (Figure 6) in the studied veins suggest that the involved hydrothermal fluids of the Jandaq oceanic crust were leached the calcic plagioclase-rich lithologies as pillow lavas, diabasic sheeted dykes and gabbroic lithologies before penetrating the lower crust.

The formation of diopsidites (Python et al., 2007 a,b; 2011; Akizawa and Arai, 2014) and hornblendite (Torabi et al., 2017) in the uppermost mantle section and crustal diopsidites (Akizawa et al., 2011) in the lower crust provide useful informations about the deep circulation of seawater-derived fluids at high temperature hydrothermal activity. This circulation changes the primary distribution of Ca, Si, Eu and REE in the crust and the upper mantle. The chemical compositions of minerals in the studied veins indicate the mobility of Ca, Si, Al, Fe, Mg and REE during activity of the seawater-derived high temperature fluids. They are gained Ca during circulation through the crustal section down to the mantle. The Mg content is lower than the other ions in the major minerals and presents only as a main component in the clinopyroxenes suggest a lower activity of Mg in the penetrating fluids, and point to the higher contribution of gabbros in the hydrothermal metasomatism compared to the peridotites. Accordingly, the studied hydrothermal vein-filling minerals are the results of the high temperature penetration and circulation of the seawater-derived fluids into the upper part of the oceanic crust, which is constructed of the highly porous and permeable volcanic (pillow lavas), sub-volcanic (sheeted dykes) and plutonic (tectonized and crushed gabbros) rocks.

CONCLUSIONS

Polymineralic hydrothermal veins occur within the Jandaq Paleozoic ophiolite metagabbros. The chemical compositions and the modal abundance of minerals in these veins (calcite> prehnite> garnet> epidote> clinopyroxene> chlorite> albite> sericite) show that Ca, Si, Al, Fe and Mg were the main components of involved hydrothermal fluid. High abundance of the calcite present in the mineral association of the veins indicates high fCO_2 in the hydrothermal fluid. Chemical characteristics of the minerals in the hydrothermal veins and contact zone show a systematic enrichment of the fluid mobile elements (e.g., LREE, Eu). Enrichment of Ca and Eu show that the hydrothermal fluid in the Jandaq oceanic crust was leached the basic lithologies rich in plagioclase before penetrating the lower crust. The composition of the rock-forming minerals and non-magmatic chemical signatures of the hydrothermal veins and contact zones in the Jandaq metagabbros suggest that they are possibly produced by reheating of the host rock (gabbros). The studied veins suggest a model which requires to the ingression of a seawater-derived high temperature fluid into the basic rocks of the uppermost oceanic crust.

ACKNOWLEDGEMENTS

The authors thank the University of Isfahan and Kanazawa University for financial support and providing laboratory facilities. Professor Dr. Federico Lucci is gratefully acknowledged for providing useful comments on the manuscript and Professor Dr. Paolo Ballirano (Editor in chief of Periodico di Mineralogia) and Professor Dr. Alessandro Vona (Petrology Section Editor) for editorial handling.

REFERENCES

Aistov L., Melnikov B., Krivyakin B., Morozov L., 1984. Geology of the Khur Area (Central Iran). Report TE/No. 20, Geological Survey of Iran, Iran, 132 pp.

Akizawa N. and Arai S., 2014. Petrology of mantle diopsidite from Wadi Fizh, northern Oman ophiolite: Cr and REE mobility by hydrothermal solution. Island Arc 23, 312-323.

Akizawa N., Arai S., Tamura A., Uesugi J., Python M., 2011. Crustal diopsidites from the northern Oman ophiolite: evidence for hydrothermal circulation through suboceanic Moho. Journal of Mineralogical and Petrological Societies 106, 261-266.

Alavi M., 1991. Tectonic Map of the Middle East, 1:5,000,000.

Geological Survey of Iran, Tehran.

Almasian M., 1997. Tectonics of the Anarak area (central Iran). PhD thesis, Islamic Azad University, Science and Research Unit, Iran, 164 pp.

Alt J.C., 1995. Subseafloor processes in mid-ocean ridge hydrothermal systems. In: Seafloor hydrothermal systems, Geophysical monograph (Eds.) S.E. Humphris, R.A. Zierenberg, L.S. Mullineaux, R.E. Thomson. American Geophysical Union, Washington, 85-114.

Arai S. and Akizawa N., 2014. Precipitation and dissolution of chromite by hydrothermal solutions in the Oman ophiolite: new behavior of Cr and chromite. American Mineralogist 99, 28-34.

Bach W., Jöns N., Klein F., 2012. Metasomatism within the ocean crust. In: Metasomatism and the chemical transformation of rock, Lecture notes in earth system sciences. (Eds.): D.E. Harlov and H. Austrheim, Springer Verlag, Berlin, 253-288.

Bagheri S., 2007. The exotic Paleo-tethys terrane in Central Iran: new geological data from Anarak, Jandaq and Posht-e-Badam areas. Ph.D. Thesis, Faculty of Geosciences and Environment, Univ. Lausanne, Switzerland, 208 pp.

Bagheri S. and Stampfli G.M., 2008. The Anarak, Jandaq and Posht-e-Badam metamorphic complexes in central Iran: new geological data, relationships and tectonic implication. Tectonophysics 451, 123-155.

Balini M., Nicora A., Berra F., Garzanti E., Levera M., Mattei M., Muttoni G., Zanchi A., Bollati I., Larghi C., Zanchetta S., Salamati R., Mossavvari F., 2009. The Triassic stratigraphic succession of Nakhlak (Central Iran), a record from an active margin. In: South Caspian to Central Iran basins. (Eds.): M.F. Brunet, M. Wilmsen, J.W. Granath. Geological Society of London, Special Publication, London, UK 312, 287-321.

Berberian M. and King G.C.P., 1981. Towards a paleogeography and tectonic evolution of Iran. Canadian Journal of Earth Science 18, 210-265.

Berger J., Femenias O., Mercier J.C.C., Demaiffe D., 2005. Ocean-floor hydrothermal metamorphism in the Limousin ophiolites (western French Massif Central): evidence of a rare preserved Variscan oceanic marker. Journal of metamorphic Geology 23, 795-812.

Berra F., Zanchi A., Angiolini L., Vachard D., Vezzoli G., Zanchetta S., Bergomi M., Javadi H.R., Kouhpeyma M., 2017. The upper Paleozoic Godar-e-Siah complex of Jandaq: evidence and significance of a north Palaeo-Tethyan succession in Central Iran., Journal of Asian Earth Sciences 138, 272-290.

Besse J., Torcq F., Gallet Y., Ricou L.E., Krystyan L., Saidi A., 1998. Late Permian to late Triassic paleomagnetic data from Iran: constraints on migration of the Iranian block through the Tethyan Ocean and initial destruction of Pangea. Geophysical Journal International 135, 77-92.

Blundy J. and Wood B., 1994. Prediction of crystal-melt partition coefficients from elastic moduli. Nature 372, 452-454.

Davoudzadeh M., 1997. Geology of Iran. In: Encyclopedia of Asian and European regional geology. (Eds.) E.M. Moores and R.W. Fairbridge. Chapman & Hall, London.

Davoudzadeh M., Lensch G., Diefenbach K.W., 1986. Contribution to the paleogeography, stratigraphy and tectonics of the Infracambrian and Lower Paleozoic of Iran. Neues Jahrbuch für Geologie und Paläontologie, Abhandlungen 172, 245-269.

Deer W.A., Howie R.A., Zussman J., 1992. An introduction to the rock forming minerals. Longman, London, 528 pp.

Dick H.J.B., Natland J.H., Alt J.C., Bach W., Bideau D., Gee J.S., Haggas S., Hertogen J.G.H., Hirth G., Holm P.M., Ildefonse B., Iturrino G.J., John B.E., Kelley D.S., Kikawa E., Kingdon A., LeRoux P.J., Maeda J., Meyer P.S., Miller D.J., Naslund H.R., Niu Y., Robinson P.T., Snow J., Stephen R.A., Trimby P.W., Worm H.U., Yoshinobu A., 2000. A long in situ section of the lower ocean crust: results of ODP Leg 176 Drilling at the Southwest Indian Ridge. Earth and Planetary Science Letters 179, 31-51.

Droop G.T.R., 1987. A general equation for estimating Fe^{3+} concentrations in ferromagnesian silicates and oxides from microprobe analyses, using stoichiometric criteria. Mineralogical Magazine 51, 431-435.

Frost B.R., Beard J.S., McCraig A., Condliffe E., 2008. The formation of micro-rodingites from IODP Hole U1309D: Key to understanding the process of serpentinization. Journal of Petrology 49, 1579-1588.

Ferry J.M. and Dipple G.M.,1991. Fluid flow, mineral reactions, and metasomatism. Geology 19, 211-214.

Gillis K.M., 1995. Controls on hydrothermal alteration in a section of fast-spreading oceanic crust. Earth and Planetary Science Letters 134, 473-489.

Gillis K.M. and Meyer P.S., 2001. Metasomatism of oceanic gabbros by late stage melts and hydrothermal fluids: evidence from the rare earth element composition of amphiboles. Geochemistry, Geophysics, Geosystems 2(3). doi: 10.1029/2000GC000087.

Harris M., Coggon R.M., Smith-Duque C.E., Cooper M.J., Milton J.A., Teagle D.A.H, 2015. Channelling of hydrothermal fluids during the accretion and evolution of the upper oceanic crust: Sr isotope evidence from ODP Hole 1256D. Earth and Planetary Science Letters 416, 56-66.

Hawthorne F.C., Oberti R., Harlow G.E., Maresch W.V., Martin R.F., Schumacher J.C., Welch M.D., 2012. Nomenclature of the amphibole supergroup. American Mineralogist 97, 2031-2048.

Hey M.H., 1954. A new review of the chlorites. Mineralogical Magazine 30, 277-292.

Holland T. and Blundy J., 1994. Non-ideal interaction in calcic amphibole and their bearing on amphibole-plagioclase thermometry. Contributions to Mineralogy and Petrology 116, 433-447.

Huot F., Hébert R., Varfalvy V., 2002. The Beimarand mélange

(southern Tibet) brings additional constraints in assessing the origin, metamorphic evolution and obduction processes of the Yarlung Zangbo ophiolite. Journal of Asian Earth Science 21, 307-322.

Jamshidi-Badr M., Collins A.S., Masoudi F., Cox G., Mohajjel M., 2013. The U-Pb age, geochemistry and tectonic significance of granitoids in the Soursat Complex, Northwest Iran. Turkish Journal of Earth Sciences 22, 1-31.

Jarrard R.D., 2003. Subduction fluxes of water, carbon dioxide, chlorine, and potassium. Geochemistry, Geophysics, Geosystems 4(5): 8905. doi: 8910.1029/2002GC000392.

Kitajima K., Maruyama S., Utusnomiya S., Liou J.G., 2001. Seafloor hydrothermal alteration at an Archean midocean ridge. Journal of Metamorphic Geology 19, 583-599.

Klein M., Stosch H.G., Seck H.A., 1997. Partitioning of high field-strength and rare-earth elements between amphibole and quartz-dioritic to tonalitic melts: An experimental study. Chemical Geology 138, 257-271.

Lieftink D.J., Nijland T.G., Maijer C., 1994. The behavior of rare-earth elements in high-temperature Cl-bearing aqueous fluids: Results from the Ødegårdens verk natural laboratory. The Canadian Mineralogist 32, 149-158.

Liou J.G., Kim H.G., Maruyama S., 1983. Prehnite-epidote equilibria and their petrologic applications. Journal of Petrology 24, 321-342.

Lippard S.J., Shelton A.W., Gass I.G., 1986. The ophiolites of northern Oman. Geological Society of London, 178 pp.

McCollom T.M. and Shock E.L., 1998. Fluid-rock interactions in the lower oceanic crust: thermodynamic models of hydrothermal alteration. Journal of Geophysical Research 103, 547-575.

McDonough W.F. and Sun S.S., 1995. The composition of the earth. Chemical Geology 120, 223-253.

Morimoto N., 1989. Nomenclature of pyroxenes. The Canadian Mineralogist 27, 143-156.

Morishita T., Ishida Y., Arai S., 2005. Simultaneous determination of multiple trace element compositions in thin (<30 μm) layers of BCR-2G by 193 nm ArF excimer laser ablation-ICP-MS: implications for matrix effect and elemental fractionation on quantitative analysis. Geochemical Journal 39, 327-340.

Muttoni G., Mattei M., Balini M., Zanchi A., Gaetani M., Berra F., 2009. The drift history of Iran from the Ordovician to the Triassic. Geological Society of London 312, 7-29.

Nicolas A., Mainprice D., Boudier F., 2003. High-temperature seawater circulation throughout crust of oceanic ridges: a model derived from the Oman ophiolites. Journal of Geophysical Research 108, 1-20.

Nosouhian N., Torabi G., Arai S., 2014. Metapicrites of the Bayazeh ophiolite (Central Iran), a trace of Paleo-Tethys subduction-related mantle metasomatism. Neues Jahrbuch für Geologie und Paläontologie, Abhandlungen 271, 1-19.

Nosouhian N., Torabi G., Arai S., 2016. Amphibole-bearing listwaenites from the Paleozoic Bayazeh ophiolite (Central Iran). Italian Journal of Geosciences 135, 109-119.

Nosouhian N., Torabi G., Arai S., 2019. Petrological aspects of the Bayazeh Paleozoic ophiolite (Central Iran); implications for Paleo-Tethys subduction. Periodico di Mineralogia 88, 155-184.

Otten M.T., 1984. The origin of brown hornblende in Artfjallet gabbro and dolerites. Contribution to Mineralogy and Petrology 86, 189-199.

Python M., Ceuleneer G., Ishida Y., Barrat J.A., Arai S., 2007a. Oman diopsidites: a new lithology diagnostic of very high temperature hydrothermal circulation in mantle peridotite below oceanic spreading centres. Earth and Planetary Science Letters 255, 289-305.

Python M., Ishida Y., Ceuleneer G., Arai S., 2007b. Trace element heterogeneity in hydrothermal diopside: evidence for Ti depletion and Sr-Eu-LREE enrichment during hydrothermal metamorphism of mantle harzburgite. Journal of Mineralogical and Petrological Societies 102, 143-149.

Python M., Yoshikawa M., Shibata T., Arai S., 2011. Diopsidites and rodingites: Serpentinisation and Ca-Metasomatism in the Oman ophiolite mantle. In: Dyke swarms: Keys for geodynamic interpretation. (Eds.) K. Srivastava. Springer, Verlag Berlin Heidelberg, 605 pp.

Puga E., Nieto J.M., Dias de Frederico A., Bodinier J.L., Morten L., 1999. Petrology and metamorphic evolution of ultramafic rocks and dolerite dykes of the Betic Ophiolitic Association (Mulhacén Complex, SE Spain): evidence of eo-Alpine subduction following an ocean-floor metasomatic process. Lithos 49, 23-56.

Reichert J., 2007. A metallogenetic model for carbonate-hosted non-sulphide zinc deposits based on observations of Mehdi Abad and Irankuh, central and southwestern Iran. Ph.D. Thesis, Martin-Luther University, Halle-Wittenberg, 157 pp.

Rossetti F., Nozaem R., Lucci F., Vignaroli G., Gerdes A., Nasrabadi M., Theye T., 2015. Tectonic setting and geochronology of the Cadomian (Ediacaran-Cambrian) magmatism in Central Iran, Kuh-e-Sarhangi region (NW Lut Block). Journal of Asian Earth Sciences 102, 24-44.

Rossetti F., Monie P., Nasrabady M., Theye T., Lucci F., Saadat M., 2017. Early Carboniferous subduction-zone metamorphism preserved within the Palaeo-Tethyan Rasht ophiolites (western Alborz, Iran). Journal of the Geological Society 174, 741-758.

Rutherford M.J., Sigurdsson H., Carey S., Davis A., 1985. The May 18, 1980, eruption of Mount St. Helens: 1. Melt composition and experimental phase equilibria. Journal of Geophysical Research 90, 2929-2947.

Sato H., Nakada S., Fujii T., Nakamura M., Suzuki-Kamata K., 1999. Groundmass pargasite in the 1991-1995 dacite of Unzen volcano: phase stability experiments and volcanological implications. Journal of Volcanology and Geothermal Research 89, 197-212.

Schmidt M.W., 1992. Amphibole composition in tonalite as a

function of pressure: an experimental calibration of the Al-in-hornblende barometer. Contributions to Mineralogy and Petrology 110, 304-310.

Shafaii Moghadam H. and Stern R.J., 2014. Ophiolites of Iran: Keys to understanding the tectonic evolution of SW Asia: (I) Paleozoic ophiolites. Journal of Asian Earth Sciences 91, 19-38.

Shafaii Moghadam H., Li Q.L., Griffin W.L., Stern R.J., Ishizuka O., Henry H., Lucci F., O'Reilly S.Y., Ghorbani G., 2020. Repeated magmatic buildup and deep "hot zones" in continental evolution: the Cadomian crust of Iran. Earth and Planetary Science Letters 531(16), 1-16.

Sisson T.W. and Layne G.D., 1993. H_2O in basalt and basaltic andesite glass inclusions from four subduction-related volcanoes, Earth and Planetary Science Letters 117, 619-635.

Sisson T.W. and Grove T.L., 1993. Temperatures and H_2O contents of low-MgO high-alumina basalts, Contribution to Mineralogy and Petrology 113, 167-184.

Sobolev A.V. and Chaussidon M., 1996. H_2O concentration in primary melts from supra-subducion zones and mid-ocean ridges: implications for H_2O storage and recycling in the mantle, Earth and Planetary Science Letters 137, 45-55.

Stampfli G.M., 2000. Tethyan oceans. In: Tectonics and magmatism in Turkey and surrounding area. (Eds.) E. Bozkurt, G.A. Winchester, G.D.A. Piper. Geological Society of London, Special Publication, 1-23.

Staudigel H., Plank T., While B., Schmincke H.U., 1996. Geochemical fluxes during seafloor alteration of the basaltic upper oceanic crust: DSDP Sites 417 and 418. In: Subduction top to bottom, 96, Geophysical monograph. G.E. Bebout, D.W. Scholl, S.H. Kirby, J.P. Platt. American Geophysical Union, Washington, DC, 19-38.

Sun S.S. and McDonough W.F., 1989. Chemical and isotopic systematics of oceanic basalts: implications for mantle composition and processes. In: Magmatism in ocean basins. (Eds.) A.D. Saunders and M.J. Norry. Geological Society Special Publication 42, 313-345.

Takin M., 1972. Iranian geology and continental drift in the Middle East. Nature 235, 147-150.

Torabi G., 2011. Late Permian blueschist from Anarak ophiolite (Central Iran, Isfahan province), a mark of multi-suture closure of the Paleo-Tethys ocean. Revista Mexicana de Ciencias Geológicas 28, 544-554.

Torabi G. and Arai S., 2013. Back-arc Paleo-Tethys related blueschist from Central Iran (South of Chupanan, Isfahan Province). Petrology 21, 393-407.

Torabi G., Arai S., Koepke J., 2011. Metamorphosed mantle peridotites from Central Iran (Jandaq area, Isfahan province). Neues Jahrbuch für Geologie und Paläontologie, Abhandlungen 261, 129-150.

Torabi G., Arai S., Morishita T., Tamura A., 2017. Mantle Hornblendites of Naein Ophiolite (Central Iran): Evidence of Deep High Temperature Hydrothermal Metasomatism in an Upper Mantle Section. Petrology 25, 114-137.

Van Hinsbergen D.J.J., Peters K., Maffione M., Spakman W., Guilmette C., Thieulot C., Plumper O., Gurer D., Brouwer F.M., Aldanmaz E., Kaymakcı N., 2015. Dynamics of intraoceanic subduction initiation: 2. Suprasubduction zone ophiolite formation and metamorphic sole exhumation in context of absolute plate motions. Geochemistry, Geophysics, Geosystems 16, 1771-1785.

Webster J.D., 1992. Water solubility and chlorine partitioning in Cl-rich granitic systems: effects of melt composition at 2 kbar and 800 °C. Geochimca et Cosmochimica Acta 56, 679-687.

Wendt J., Kaufmann B., Belka Z., Farsan N., Karimi Bavandpour A.R., 2005. Devonian/Lower Carboniferous stratigraphy, facies patterns and palaeogeography of Iran, part II. Northern and Central Iran. Acta Geologica Polonica 55, 31-97.

Whitney D.L. and Evans B.W., 2010. Abbreviations for names of rock-forming minerals. American Mineralogist 95, 185-187.

Wones D.R., 1989. Significance of the assemblage titanite + magnetite + quartz in granitic rocks. American Mineralogist 74, 744-749.

Zanchi A., Zanchetta S., Garzanti E., Balini M., Berra F., Mattei M., Muttoni G., 2009. The Cimmerian evolution of the Nakhlak-Anarak area, Central Iran, and its bearing for the reconstruction of the history of the Eurasian margin. Geological Society of London 312, 261-286.